Molecular Symmetry Properties of Conical Intersections and Nonadiabatic Coupling Terms: Theory and Quantum Chemical Demonstration for Cyclopenta-2,4-dienimine (C_5H_4NH)[†]

S. Al-Jabour,[‡,§] M. Baer,[||] O. Deeb,[§] M. Leibscher,[*,‡] J. Manz,[‡] X. Xu,[⊥] and S. Zilberg[⊥]

Institut für Chemie und Biochemie, Freie Universität Berlin, Germany, Faculty of Pharmacy, Al-Quds University, Palestine, The Fritz Haber Center for Molecular Dynamics, The Hebrew University of Jerusalem, Israel, and Department of Physical Chemistry and the Farkas Center for Light Induced Processes, The Hebrew University of Jerusalem, Israel

Received: May 29, 2009; Revised Manuscript Received: August 6, 2009

This paper discovers molecular symmetry (MS) properties of conical intersections (CIs) and the related nonadiabatic coupling terms (NACTs) in molecules which allow large amplitude motions such as torsion, in the frame of the relevant molecular symmetry group, focusing on groups with one-dimensional (1-d) irreducible representations (IREPs). If one employs corresponding MS-adapted nuclear coordinates, the NACTs can be classified according to those IREPs. The assignment is supported by theorems which relate the IREPs of different NACTs to each other, and by properties of the NACTs related to the CIs. For example, planar contour integrals of the NACTs evaluated along loops around the individual CIs are equal to $+\pi$ or $-\pi$, depending on the IREP-adapted signs of the NACTs. The + or − signs for the contour integrals may also be used to define the "charges" and IREPs of the CIs. We derive various general molecular symmetry properties of the related NACTs and CIs. These provide useful applications; e.g., the discovery of an individual CI allows one to generate, by means of all molecular symmetry operations, the complete set of CIs at different symmetry-related locations. Also, we show that the seams of CIs with different IREPs may have different topologies in a specific plane of MS-adapted coordinates. Moreover, the IREPs impose symmetrical nodes of the NACTs, and this may support their calculations by quantum chemical *ab initio* methods, even far away from the CIs. The general approach is demonstrated by application to an example. Specifically, we investigate the CIs and NACTs of cyclopenta-2,4-dienimine (C_5H_4NH) which has C_{2v}(M) molecular symmetry with 1-d IREPs. The results are confirmed by quantum chemical calculations, starting from the location of a CI based on the Longuet-Higgins phase change theorem, until a proof of self-consistency, i.e., the related symmetry-adapted NACTs fulfill quantization rules which have been derived in [Baer, M. *Beyond Born−Oppenheimer: Electronic non-Adiabatic Coupling Terms and Conical Intersections*; Wiley & Sons Inc.: Hoboken, NJ, 2006].

I. Introduction

The purpose of this paper is to discover molecular symmetry (MS) properties of conical intersections (CIs) and the related nonadiabatic coupling terms (NACTs) in molecules which allow large amplitude motions such as torsion, in the frame of the relevant molecular symmetry group, focusing on groups with one-dimensional (1-d) irreducible representations (IREPs). This goal is not only of fundamental interest, but it is also important for applications; e.g., we shall show that the discovery of an individual CI and the assignment of its IREP generate automatically the complete set of analogous CIs at symmetry-related locations. Moreover, the CIs and NACTs, which appear in the Born−Oppenheimer expansion of the Schrödinger equation,[1] determine the nonadiabatic processes, e.g., for the photochemistry of the given system;[2,3] see also ref 4; knowledge of the symmetry properties should thus be important for adequate predictions of the nonadiabatic reaction dynamics, including interferences. Here, we do not mean necessarily the Aharonov−Bohm effect as frequently discussed in the literature[5−7] but more general molecular-symmetry-related effects of interferences. In particular, we shall show that the seams of CIs with different IREPs may have different topologies in a specific plane of MS-adapted coordinates, implying different nonadiabatic processes. Last but not least, the molecular symmetries impose symmetric nodes on the NACTs, depending on their IREPs; we shall also show that this may assist quantum chemical calculations of the NACTs, specifically in domains far away from conical intersections where the absolute values of the NACTs may drop possibly below the level of accuracy of the applied method of quantum chemistry. In such cases, the symmetry properties of the NACTs determine their relative signs in analogous symmetry-related locations, even far away from each other. Traditional quantum chemistry cannot provide that information *per se*, because it is designed as a method for determining the electronic structures in local domains of nuclear coordinates, e.g., close to equilibrium structures of reactants or products, or transition states, with corresponding assignments of IREPs for the molecular point group of the system; this is quite different from the molecular symmetry group which *nomen est omen* accounts for the global molecular symmetry properties, in all accessible geometries. Our approach invokes a number of steps which are listed below as a work plan:

[†] Part of the "Benoît Soep Festschrift".

* Corresponding author. E-mail: monika@chemie.fu-berlin.de.
[‡] Freie Universität Berlin.
[§] Al-Quds University.
[||] The Fritz Haber Center for Molecular Dynamics, The Hebrew University of Jerusalem.
[⊥] Department of Physical Chemistry and the Farkas Center for Light Induced Processes, The Hebrew University of Jerusalem.

10.1021/jp905038t
Published on Web 11/06/2009

(i) the assignment of the molecular symmetry (MS) of the given system which may undergo large amplitude motion, e.g., torsion, cf. ref 8, and considerations of the consequences, e.g., applications of the molecular symmetry operations in order to construct sets of analogous symmetry-related geometries, and a discussion of the difficulties to assign molecular IREPs to electronic states,

(ii) the definition of corresponding symmetry-adapted nuclear coordinates and their derivatives which should transform as the IREPs of the MS group, for small as well as large amplitude motions,

(iii) the expression of the CIs and the corresponding seams[2] of the CIs in terms of these coordinates,

(iv) the definition of the related NACTs using the symmetry-adapted coordinates,

(v) the derivation of two theorems which relate the IREPs of different NACTs to each other,

(vi) the determination of symmetric nodes of the NACTs, together with the (relative) signs of the NACTS in different symmetry-related domains, even far away from the CIs,

(vii) the assignment of IREPs to the NACTs, by means of the two general theorems as well as by three well-known properties of the NACTs related to the CIs. Specifically, we shall employ the so-called quantization rule for the NACTs,[1] the pole property of the NACTs close to the CIs,[1,2] and the fact that the electronic wave functions for the two states which become degenerate at a CI may change characters close to the CIs, with consequences for the NACTs. Further details will be specified below; see eqs 22−27 in section II. Here, it is sufficient to say that these properties have been documented previously, mainly for small molecules, i.e., tri- and tetra-atomic molecules, without considerations of large amplitude motions which call for molecular symmetry groups.[1,2,9−27] An approach based on an *ab initio* treatment[1,28,29] was recently extended to a larger system, CH_3NH_2.[30]

(viii) the definition of corresponding signs or "charges" of the symmetry-related CIs,

(ix) the assignment of the corresponding IREPs of the CIs,

(x) the derivation of different topologies of the seams of the CIs depending on their molecular symmetries in a specific plane of MS-adapted coordinates.

While this work plan (i−x) should be applicable to arbitrary molecules which undergo small as well as large amplitude motions which transform according to 1-d IREPs of the MS group, they will be explained and demonstrated for a specific example, i.e., cyclopenta-2,4-dienimine (C_5H_4NH). For example, in step i, we shall determine its molecular symmetry group, etc. This allows us to illustrate a number of additional consequences of the MS for the NACTs and CIs including

(xi) the support of quantum chemistry calculations of the NACTs in domains far away from the CIs and, last but not least,

(xii) tests of self-consistency; e.g., the symmetry-adapted NACTs satisfy quantization rules which have been derived previously by one of us.[1]

The chosen model system C_5H_4NH is challenging because it is a rather large (compared to the above-mentioned models) exocyclic analogue of methylene-imine (CH_2NH), the parent molecule with a C═N double bond, which provides two different reaction pathways from the planar syn configuration of the reactant along large amplitude motions via three different transition states to the planar anti configurations of the product,[31] pointing to possibly rich and instructive scenarios of various conical intersections. For the purpose of a proof of principle, the present investigation of the symmetry properties of C_5H_4NH will be restricted to just three electronic states: first, the electronic ground state S_0 which has a potential minimum for the planar syn configuration. At this special configuration, traditional quantum chemistry assigns the notation $S_0 = 1A'$, according to the "local" IREP A' of the corresponding molecular point group C_s (NOT to be mixed up with global molecular symmetry.) Moreover, we include the next two excited singlet states which have (local) A' symmetry, $S_1 = 2A'$ and $S_2 = 3A'$. Since we aim at describing large amplitude motions, i.e., torsion, we shall not employ the notation for the "local" symmetry. Instead, we shall use the "global" notation S_j, with $j = 0$, 1, and 2 which indicates the energetic order of the adiabatic potentials V_j.

The double goal of the general derivations and the verifications by means of quantum chemistry calculations for the model system C_5H_4NH should provide significant extensions of the theory for the NACTs and CIs, beyond the quoted previous investigations. The work plan (i−x) will be carried out in section II. The results will be confirmed by quantum chemical calculations, starting from the location of a conical intersection of state S_0 and S_1 based on the Longuet-Higgins phase change theorem;[32,33] see also refs 34−36 until items xi and xii; see section III. The conclusions are in section IV.

II. Theory with an Example

A. Assignment of the Molecular Symmetry Group. According to the work-plan of section I, our derivation starts with

(i) the assignment of the molecular symmetry group of the given system, allowing large amplitude motion, e.g., torsion, cf. ref 8, focusing on groups with 1-d IREPs. The group MS consists, in general, of G symmetry operations $\hat{S}_g$, with $g = 1$, 2, ... , G, including the identity $\hat{S}_1 = E$, all feasible permutations P of the spatial and spin coordinates of equivalent nuclei, and possibly the inversion E^* of all nuclear coordinates s and electronic coordinates s_e, and the inversion-permutations $P \circ E^*$; specific choices of symmetry-adapted coordinates will be made below; see item ii. Application of the symmetry operations to a specific set of values (written with square brackets), say, s, $s_e = [s, s_e]_1$, generates a set of other values of the coordinates

$$[s, s_e]_g = \hat{S}_g[s, s_e]_1 \quad \text{with} \quad g = 1, 2, \ldots, G \tag{1}$$

These will be called "symmetry-related" (sets of values of) coordinates. They may be far away from each other. Nevertheless, the large amplitude motions may provide feasible paths from nuclear coordinates $[s]_1$ to the symmetry-related ones $[s]_g$.

Accordingly, the molecular symmetry group possesses G IREPs denoted as Γ_g, with $g = 1, \ldots, G$, say, $\Gamma_1 = A_1$, $\Gamma_2 = A_2$, $\Gamma_3 = B_1$, etc., with associated characters $\chi_{g,h}$ and symmetry projection operators $\hat{P}^{\Gamma_g}$. For 1-d IREPs,

$$\hat{P}^{\Gamma_g} = \frac{1}{G}\sum_h \chi_{g,h}\hat{S}_h \tag{2}$$

These $\hat{P}^{\Gamma_g}$ commute with each other, and with the total Hamiltonian $H = T_{nu} + H_{el}$ of the system, where T_{nu} is the nuclear kinetic energy operator and H_{el} is the electronic Hamiltonian. Moreover, they commute also with H_{el}. As a consequence, the (real-valued) electronic eigenfunctions $\psi_j(s_e; s)$ of H_{el}

$$H_{el}\psi_j(s_e; s) = V_j(s)\psi_j(s_e; s) \quad (3)$$

and the electronic energies, i.e., the adiabatic potential energy surfaces (PESs) $V_j(s)$ are also labeled by the IREPs Γ_g, at least in principle. In fact, the IREPs may be assigned even if the $\psi_j(s_e; s)$ accumulates a so-called topological (Berry) phase when it is transported along a closed contour around a CI,[37] thus changing its sign.[33] In practice, it may be exceedingly difficult, however, to determine the IREPs of the $\psi_j(s_e; s)$, because this would require calculation of the relative (same or opposite) signs of the ψ_j at all of the symmetry-related coordinates $[s, s_e]_g$. Due to the invariance of H_{el} with respect to $\hat{S}_g$, quantum chemistry packages would indeed yield the same absolute values of the wave functions

$$|\psi_j([s, s_e]_1)| = |\psi_j([s, s_e]_2)| = ... = |\psi_j([s, s_e]_G)| \quad (4)$$

but the relative signs of $\psi_j([s, s_e]_g)$ are not provided automatically. This deficit is due to the fact that different domains close to the symmetry-related $[s, s_e]_g$ with large values of $|\psi_j([s, s_e]_g)|$ may be separated by rather large domains where the absolute values of the $|\psi_j([s, s_e]_g)|$ may drop even below the level of accuracy of the quantum chemical method. This may be due to two reasons, with opposite consequences for the relative signs of the $\psi_j([s, s_e]_g)$: either symmetric nodes which imply a change of sign or just tunneling, without any change of sign. Quantum chemistry may fail to discriminate these cases; i.e., in practice, it may be impossible to assign the relative signs of $\psi_j([s, s_e]_g)$, but then it is also impossible to assign their IREPs!

As a resume, one should appreciate the advantage but also recognize the deficit of (*ab initio*) quantum chemistry methods concerning the assignments of IREPs to electronic wave functions: this is now routine for molecular point groups, but it may be inefficient concerning the molecular symmetry group. This shortcoming provides the particular motivation or challenge that we address in this paper, i.e., to develop the approach which allows one to assign IREPs to the NACTs and CIs, even if the IREPs of the ψ's are not known. Indeed, the subsequent derivations of the symmetry properties of the NACTs do not even require that one evaluates those $\psi_j(s_e; s)$ and $V_j(s)$ explicitly. In practice, we restrict the investigation to a finite number of electronic states, typically the electronic ground and few excited states, with the same spin multiplicity (neglecting effects of spin−orbit couplings), say, S_0, S_1, ... , S_j, ... , $S_{j_{max}}$.

By analogy with relation 4, if one discovers a conical intersection, say, for the nuclear coordinates $s = [s]_1$, then one can apply all the symmetry operations $\hat{S}_g$ of the molecular symmetry group to $[s]_1$ in order to generate a complete set of CIs which are located at the corresponding set of symmetry-related values of the coordinates $[s]_g = \hat{S}_g[s]_1$. Subsequently (see step iii), this procedure will be applied using symmetry-adapted coordinates (see step ii). Likewise, if any property of the NACTs is determined at another value of the nuclear coordinates, say, $[s]'_1$, then analogous properties of the NACTs are predicted at all symmetry-related coordinates $[s]'_g = \hat{S}_g[s]'_1$.

As an example, Figure 1a shows the molecule cyclopenta-2,4-dienimine (C_5H_4NH), which allows large amplitude motion, i.e., torsion of the hydrogen atom of the NH bond around the axis which is defined by the CN bond. Figure 1a also illustrates the effects of the four molecular symmetry operations, i.e., the identity E, the inversion E^*, the simultaneous permutation (12) of the coordinates of the four nuclei of one of the fragments H—C═C—H (labeled "1") of the cyclopenta-2,4-dienyl ring with the opposite one (labeled "2"), and the inversion permutation $(12)^* = (12)\circ E^*$. The model C_5H_4NH does not allow any other feasible permutations of the nuclei. Hence, the four ($G = 4$) symmetry operations $\hat{S}_1 = E$, $\hat{S}_2 = (12)$, $\hat{S}_3 = E^*$, and $\hat{S}_4 = (12)^*$ constitute the molecular symmetry group $C_{2v}(M)$. The notation "(M)" stands for the molecular symmetry. The MS group $C_{2v}(M)$ is isomorphic to the molecular point group C_{2v}, with corresponding IREPs A_1, A_2, B_1, and B_2. The character table

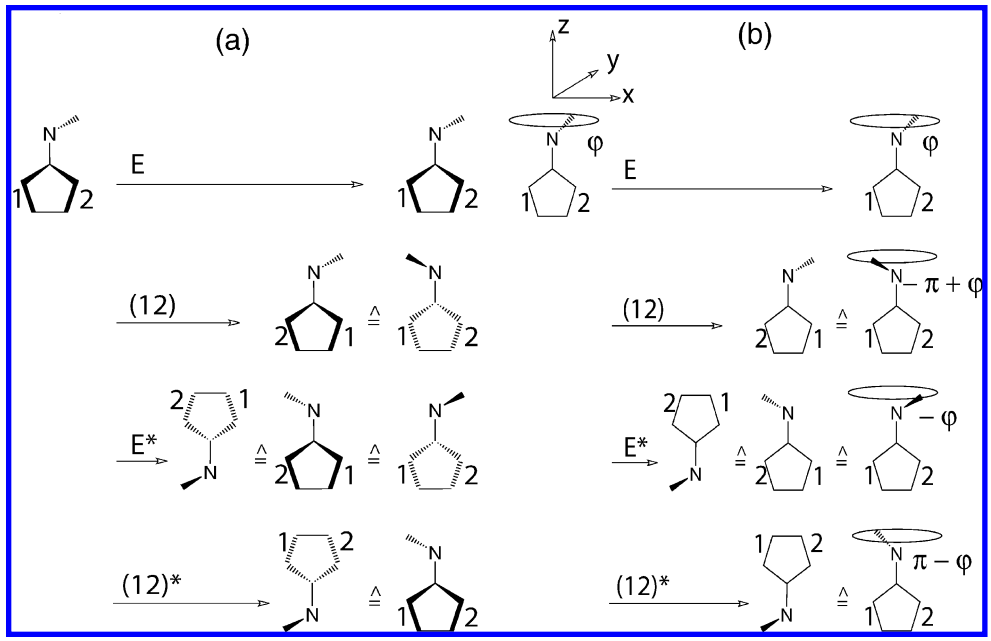

Figure 1. Effects of the four symmetry operations E, (12), E^*, and $(12)^*$ of the molecular symmetry group $C_{2v}(M)$ on the model system, cyclopenta-2,4-dienimine (C_5H_4NH), with arbitrary configurations (panel a, courtesy of Prof. D. Haase), and with constraints to planar fragment C_5H_4N with C_{2v} molecular point group symmetry (panel b, see text). The ring-type trajectory in panel b illustrates the torsion of the NH bond along the torsional angle φ and with constant radius r. The effects of the symmetry operations on φ are also illustrated in panel b (cf. Table 1), while r remains unaffected. The example is for the case $0 \le \varphi \le \pi/2$, such that all of the symmetry-adapted angles are in the domain $[-\pi, \pi]$. Also shown are the orientations of the x- and y-axes for the related coordinates $x = r\cos\varphi$ and $y = r\sin\varphi$.

TABLE 1: Character Table of the Molecular Symmetry Group C_{2v}(M) of C_5H_4NH, with Extensions, see Figure 1[a–f]

$C_{2v}(M)$[(a)] $\hat{S}_g$	E $\hat{S}_1$	(12) $\hat{S}_2$	E* $\hat{S}_3$	(12)* $\hat{S}_4$	coord. (rotation)	deriv.	rel. signs and nodes[(b)]	(c) 1st	2nd	3rd	4th
A_1	1	1	1	1	r	$\partial/\partial r$	+ | + / + | +	τ_ϕ	τ_r	τ_x	τ_y
A_2	1	1	-1	-1	ϕ ($\hat{R}_\phi$)	$\partial/\partial\phi$	− ‖ + / + ‖ −	τ_r	τ_ϕ	τ_y	τ_x
B_1	1	-1	1	-1	y	$\partial/\partial y$	+ | + = − | −	τ_x	τ_y	τ_ϕ	τ_r
B_2	1	-1	-1	1	x	$\partial/\partial x$	− ‖ + / − | +	τ_y	τ_x	τ_r	τ_ϕ
application to C_5H_4NH								−	τ_k^{12}	τ_k^{01} τ_k^{02}	−
$(r,\phi) \rightarrow \hat{S}_g(r,\phi)$ $(x,y) \rightarrow \hat{S}_g(x,y)$	(r,ϕ) (x,y)	$(r,-\pi+\phi)$ $(-x,-y)$	$(r,-\phi)$ $(x,-y)$	$(r,\pi-\phi)$ $(-x,y)$	(d) (e)						
sym.-related locations $\hat{S}_g(x,y)$	* | / | *	* / * |	* | / | *	* / * |	(f)						

[a] Isomorphic to the molecular point group C_{2v}. [b] For ψs, NACTs or CIs at $\hat{S}_g(x,y)$; see footnote [e]; the + and − signs or charges denote same and opposite relative signs, respectively; horizontal and vertical double lines indicate nodes at the x and y axis, respectively. [c] Four possible combinations of IREPs of the NACTs. The short-hand notation τ_k denotes the NACT τ_k^{ij} for unspecified electronic states i and j, with respect to the derivative for the nuclear coordinates $s_k = r$, φ, x, or y. Applications of the second and third possible combinations for the NACTs of C_5H_4NH are specified below. [d] Effects of the symmetry operations $\hat{S}_g$ yielding symmetry-related molecular structures with the same radius r but different torsional angles, cf. Figure 1b and eq 1. [e] Effects of the symmetry operations $\hat{S}_g$ yielding symmetry-related molecular structures with different Cartesian coordinates, cf. eq 5. [f] Symmetry-related top right, bottom left, bottom right, and top left locations correspond to $\hat{S}_g(x,y)$ with $g = 1$, 2, 3, and 4, respectively.

of C_{2v}(M) is shown in Table 1. The subsequent investigation will be restricted just to the three lowest singlet states S_j, $j = 0$, 1, 2, of the model C_5H_4NH.

B. Molecular-Symmetry-Adapted Coordinates. (ii) Next, we define corresponding sets of molecular-symmetry-adapted nuclear coordinates (denoted by curly brackets) $s = \{s_k\}$, together with the $\partial/\partial s_k$ derivatives. These should transform as the IREPs of the MS group, and they should allow one to describe the characteristic large amplitude motions of the molecular, as well as vibrations with small amplitudes. In principle, accurate presentations of all coupled vibrations and rotations of a nonlinear moleculer with N_{nu} nuclei would call for $3N_{nu} - 3$ coordinates s_k, subtracting three coordinates for the motion of the molecular center of mass. Subsequently, we assume that the molecule is in the rotational ground state such that the wave function does not depend on the rotational Euler angles. All of the subsequent results are valid, therefore, for arbitrary reorientations of the molecule; this assumption has been used implicitly for the molecular rotation which is illustrated in Figure 1. For simplicity, one may also employ models of reduced dimensionality, with explicit considerations of a smaller number of molecular-symmetry-adapted coordinates s_k, $k = 1$, 2, ... , n (including those which account for the large amplitude motions) while freezing the other ones. The derivation of the molecular Hamiltonian in reduced dimensionality has been explained in refs 4 and 29. These types of n-dimensional (n-d) models imply constraints on the molecular geometries; e.g., they may describe configurations which are close to but not automatically exactly equal to the equilibrium structures of the reactants and products, transition states, conical intersections, or any other structures of reference, and corresponding large amplitude motions between these configurations. It depends on the purpose of the specific investigation whether the model of reduced dimensionality suffices to provide, say, satisfactory semiquantitative results, or whether one prefers to include additional degrees of freedom for higher accuracy, at the expense of higher computational demands.

For the present purpose which aims at a demonstration of the principles of molecular symmetry properties of the CIs and NACTs, we employ just two symmetry-adapted coordinates, $s = \{s_1, s_2\}$ of the model system C_5H_4NH, while freezing the other $3 \times 11 - 3 - 2 = 28$ ones. Specifically, the fragment C_5H_4N including the CN bond and the cyclopentadienyl ring is frozen in a planar configuration corresponding to local C_{2v} molecular point group symmetry for this molecular fragment, as shown in Figure 1b. The specific geometry of the frozen C_5H_4N fragment is irrelevant for the general derivations; a special choice will be made below in section III for the subsequent illustrations. The chosen symmetry-adapted coordinates are $s_1 = r$ ($0 \le r \le \infty$) and $s_2 = \varphi$ ($-\pi \le \varphi \le \pi$), where the dihedral angle φ (or more precisely the associated torsional rotation operator $\hat{R}_\varphi = \partial/\partial\varphi$) describes isomerization by torsion of the NH bond around the axis which is defined by the CN bond of the frozen fragment C_5H_4NH, and r is the distance of the proton of the NH bond from this axis of torsion. Note that these restrictions of frozen coordinates imply that the configurations of the potential minima of the reactant and product are not included exactly in the domains of the polar coordinates φ and r, but we shall show that, nevertheless, the energies of the reactants, products, and the relevant conical intersections are approximated rather well, cf. section III. For convenience of the present study which aims at investigations of the global symmetries, we define φ in the domain from $-\pi$ to $+\pi$ such that $\varphi = 0$ corresponds to the planar syn configuration of the reactant, whereas $\varphi = -\pi$ or $+\pi$ corresponds to the anti configuration of the product. In C_{2v}(M) symmetry, these coordinates r and φ (or more precisely the related torsion $\hat{R}_\varphi$), as well as their derivatives $\partial/\partial r$ and $\partial/\partial\varphi$, transform as A_1 and A_2, respectively; see Table 1 and Figure

1b. Alternatively, one may also employ the related symmetry-adapted Cartesian coordinates

$$x = r\cos\varphi$$
$$y = r\sin\varphi \quad (5)$$

These and their derivatives $\partial/\partial x$ and $\partial/\partial y$ transform as B_2 and B_1, respectively, cf. Table 1. Rigorously, the Cartesian coordinates are attached to the heavy C_5H_4N fragment. The relation 5 yields the values of these coordinates depending on the values of the coordinates $\{r, \varphi\}$ which describe the motion of the light proton of the NH bond relative to C_5H_4N.

The effects of the symmetry operations E, (12), E^*, and (12)* on C_5H_4N in constrained configuration space of the two symmetry-adapted coordinates φ and r are illustrated in Figure 1b. As an example, we assume that the original or "first" configuration is specified by $[s]_1 = [\{r,\varphi\}]_1$, where $0 \le \varphi \le \pi/2$. One readily sees that this transforms into symmetry-related structures with torsional angles φ, $-\pi + \varphi$, $-\varphi$, and $\pi - \varphi$, in the domains $[0, \pi/2]$, $[-\pi, -\pi/2]$, $[-\pi/2, 0]$, $[\pi/2, \pi]$, respectively, covering the entire torsional domain from $-\pi$ to π, while keeping the radius r constant; these effects are also summarized in Table 1. For this reason, we shall investigate the symmetry properties of the NACTs and the related CIs versus arbitrary values of φ, while keeping the radius r as a free but constant parameter. For the present example, eq 1 reads

$$[\{r,\varphi\}, s_e]_1 = E[\{r,\varphi\}, s_e]_1 = [\{r,\varphi\}, s_e]$$
$$[\{r,\varphi\}, s_e]_2 = (12)[\{r,\varphi\}, s_e]_1 = [\{r, -\pi + \varphi\}, s_e]$$
$$[\{r,\varphi\}, s_e]_3 = E^*[\{r,\varphi\}, s_e]_1 = [\{r, -\varphi\}, -s_e]$$
$$[\{r,\varphi\}, s_e]_4 = (12)^*[\{r,\varphi\}, s_e]_1 = [\{r, \pi - \varphi\}, -s_e] \quad (6)$$

See Table 1, and eq 4 is specified as

$$|\psi_j([r,\varphi,s_e])| = |\psi_j([r,-\pi+\varphi,s_e])| = |\psi_j([r,-\varphi,-s_e])| = |\psi_j([r,\pi-\varphi,-s_e])| \quad (7)$$

C. Generation of Molecular-Symmetry-Related Conical Intersections. (iii) Third, the CIs and the corresponding seams of the CIs are determined using symmetry-adapted nuclear coordinates. For this purpose, eq 3 is applied using $s = \{s_k\}$, cf. item ii. For specific values $s = s^{i,i+1} = \{s_k^{i,i+1}\}$, neighboring pairs of the resulting adiabatic potentials are degenerate

$$V_i(s^{i,i+1}) = V_{i+1}(s^{i,i+1}) \quad (8)$$

Equation 8 defines the associated seam $s^{i,i+1} = \{s_k^{i,i+1}\}$ of the conical intersection, which is written with the corresponding notation $CI^{i,i+1}(s^{i,i+1})$.

Relation 1 and the molecular symmetry of the electronic Hamiltonian imply that if a conical intersection has been discovered at special values, say, $s^{i,i+1} = [s^{i,i+1}]_1 = [\{s_k^{i,i+1}\}]_1$, then one can apply all of the symmetry operations $\hat{S}_g$ to $CI_1^{i,i+1} = CI^{i,i+1}([s^{i,i+1}]_1)$, and this will generate a complete set of molecular-symmetry-related $CI_g^{i,i+1} = CI^{i,i+1}([s^{i,i+1}]_g)$ located at the

$$[s^{i,i+1}]_g = \hat{S}_g[s^{i,i+1}]_1 \quad \text{with} \quad g = 1, 2, \ldots, G \quad (9)$$

Below (see steps viii and ix), we shall define signs or "charges" $e_g^{i,i+1}$ to the set of $CI_g^{i,i+1}$, and determine the corresponding IREP of $CI^{i,i+1}$.

Accordingly, for the present example which focuses on three electronic states S_0, S_1, and S_2 of C_5H_4NH, we shall determine the conical intersections at special values of the symmetry-adapted nuclear coordinates. According to the general notation, these are denoted as $CI^{0,1}(\{r^{0,1}, \varphi^{0,1}\})$ and $CI^{1,2}(\{r^{1,2}, \varphi^{1,2}\})$, and the specific values of the coordinates of the "first" representatives $CI_1^{0,1}$ and $CI_1^{1,2}$ are $\{r^{0,1}, \varphi^{0,1}\} = [\{r^{0,1}, \varphi^{0,1}\}]_1$ and $\{r^{1,2}, \varphi^{1,2}\} = [\{r^{1,2}, \varphi^{1,2}\}]_1$, respectively. Applications of the four molecular symmetry operations $\hat{S}_g$ then automatically generate complete sets of analogous symmetry-related conical intersections, denoted $CI_g^{0,1} = CI^{0,1}([\{r^{0,1}, \varphi^{0,1}\}]_g)$ and $CI_g^{1,2} = CI^{1,2}([\{r^{1,2}, \varphi^{1,2}\}]_g)$ at symmetry-related values of coordinates $[\{r^{0,1}, \varphi^{0,1}\}]_g = \hat{S}_g[\{r^{0,1}, \varphi^{0,1}\}]_1$ and $[\{r^{1,2}, \varphi^{1,2}\}]_g = \hat{S}_g[\{r^{1,2}, \varphi^{1,2}\}]_1$, respectively.

D. Nonadiabatic Coupling Terms (NACTs) in Terms of Molecular-Symmetry-Adapted Coordinates. (iv) Fourth, using the symmetry-adapted nuclear coordinates $s = \{s_k\}$, we define the NACTs of the (real-valued) electronic wave function $\psi_i(s_e, s)$ and the $\partial/\partial s_k$ derivative of $\psi_j(s_e, s)$, integrated over the electronic coordinates s_e[1]

$$\tau_k^{i,j}(s) = \langle\psi_i(s)|\frac{\partial}{\partial s_k}\psi_j(s)\rangle = \int ds_e \psi_i(s_e, s)\frac{\partial}{\partial s_k}\psi_j(s_e, s) = -\tau_k^{j,i}(s) \quad (10)$$

with $1 \le i < j \le j_{max}$. The definition eq 10 applies to all configurations except $s = [s^{i,i+1}]_g$, i.e., away from, albeit possibly close to, the $CI^{i,i+1}([s^{i,i+1}]_g)$ where the NACTs have poles.[1] The $\tau_k^{i,j}(s)$ may be considered as components $k = 1, 2, \ldots, n$ of the vectorial NACTs, $\tau^{i,j}(s)$ for the n-d model. For reference, we note that, in principle, the IREP of the NACT eq 10 is given by

$$\Gamma(\tau_k^{i,j}) = \Gamma\left(\psi_i(s_e; s)\frac{\partial}{\partial s_k}\psi_j(s_e; s)\right) = \Gamma(\psi_i(s_e; s)) \times \Gamma\left(\frac{\partial}{\partial s_k}\right) \times \Gamma(\psi_j(s_e; s)) = \Gamma(\tau_k^{j,i}) \quad (11)$$

with $1 \le i < j \le j_{max}$. In eq 11, we use the notation $\Gamma(...)$ for IREPs of various properties, e.g., for the NACTs, the ψ's, the derivatives $\partial/\partial s_k$, etc.; analogous notations will also be applied for IREPs of other properties (...), e.g., products of NACTs or CIs. In eq 11, we have used the product theorem, focusing on 1-d irreducible representations. The third equation follows from the antisymmetry relation 10; i.e., it suffices to determine the IREPs of the $\tau_k^{i,j}$ for $i < j$. The task of determining the IREPs of the NACTs would thus be finished if the IREPs of the wave functions ψ were known for the given MS group. Since it is difficult, if not even impossible, to provide this information by means of quantum chemistry (vide infra), we shall develop an alternative approach to $\Gamma(\tau_k^{i,j})$. To begin, we note that identical absolute values of the wave functions at symmetry-related nuclear coordinates, eq 4, imply that the NACTs of (10) also have the same absolute values at symmetry-related coordinates

$$|\tau_k^{i,j}([s]_1)| = |\tau_k^{i,j}([s]_2)| = \ldots = |\tau_k^{i,j}([s]_G)| \quad (12)$$

for $1 \le i < j \le j_{max}$. Determination of the IREPs of the $\tau_k^{i,j}(s)$ will also provide their relative signs at the symmetry-related nuclear coordinates (1).

Accordingly, for the present example C_5H_4NH, we shall investigate the molecular symmetry properties of the radial and torsional NACTs $\tau_r^{0,1}$, $\tau_r^{0,2}$, and $\tau_r^{1,2}$ and $\tau_\varphi^{0,1}$, $\tau_\varphi^{0,2}$, and $\tau_\varphi^{1,2}$, respectively. The properties of the complementary NACTs $\tau_r^{1,0}$, etc., follow from the antisymmetry relation 10. It will also be useful to determine the IREPs with respect to the alternative derivatives $\partial/\partial x$ and $\partial/\partial y$; see eq 5. Relation 12 is specified as

$$\begin{aligned} |\tau_k^{i,j}([\{r,\varphi\}])| &= |\tau_k^{i,j}([\{r,-\pi+\varphi\}])| \\ &= |\tau_k^{i,j}([\{r,-\varphi\}])| = |\tau_k^{i,j}([\{r,\pi-\varphi\}])| \end{aligned} \quad (13)$$

for $i, j = 0, 1$ or $0, 2$ or $1, 2$ and $\{s_k\} = \{r,\varphi\}$ or $\{x,y\}$, together with the antisymmetry relation 10.

E. Molecular-Symmetry-Based Theorems for the NACTs. (v) Fifth, based on steps i−iv, we are now ready to derive two symmetry theorems which relate the IREPs of different NACTs to each other. Specifically, the first relation is for NACTs $\tau_k^{i,j}$ and $\tau_l^{i,j}$ with the same set of electronic states i, j but with derivatives with respect to different symmetry-adapted coordinates s_k and s_l, respectively. Relation 11 then implies that

$$\begin{aligned} \Gamma(\tau_k^{i,j}) \times \Gamma\left(\frac{\partial}{\partial s_l}\right) &= \Gamma(\psi_i(s_e;s)) \times \Gamma\left(\frac{\partial}{\partial s_k}\right) \times \Gamma(\psi_j(s_e;s)) \times \Gamma\left(\frac{\partial}{\partial s_l}\right) \\ &= \Gamma(\tau_l^{i,j}) \times \Gamma\left(\frac{\partial}{\partial s_k}\right) \end{aligned} \quad (14)$$

or

$$\Gamma(\tau_k^{i,j}) = \Gamma\left(\frac{\partial}{\partial s_k}\right) \times \Gamma\left(\frac{\partial}{\partial s_l}\right) \times \Gamma(\tau_l^{i,j}) \quad (15)$$

Theorem 15 yields the irreducible representations of all of the NACTs from the irreducible representations of a single NACT, for the same electronic states i and j, simply by multiplication with the product of the IREPs of the derivatives of the corresponding two different symmetry-adapted coordinates.

Application to the present example C_5H_4NH with molecular symmetry group $C_{2v}(M)$ allows one to set up four possible combinations of IREPs of the NACTs with respect to the derivatives of the coordinates r, φ, x, and y; these are listed in Table 1. For example, if $\Gamma(\tau_r^{i,j}) = A_1$, then theorem 15 implies that $\Gamma(\tau_\varphi^{i,j}) = A_2$, $\Gamma(\tau_x^{i,j}) = B_2$, and $\Gamma(\tau_y^{i,j}) = B_1$. Note, however, that theorem 15 does not suffice per se to decide which of the four possible combinations apply to a given set of electronic states i and j. Table 1 already anticipates that $\tau_k^{1,2}$ transforms according to the second combination, whereas $\tau_k^{0,1}$ and $\tau_k^{0,2}$ transform according to the third one, but these assignments require additional steps; see below.

The second symmetry theorem relates the IREPs of NACTs for the derivatives with respect to the same symmetry-adapted coordinate $\partial/\partial s_k$ but for different electronic states to each other. For this purpose, let us consider a loop-type sequence of N_{loop} molecular states with the same spin multiplicity, e.g., singlet states S_a, S_b, S_c, ... , S_y, $S_z = S_a$, i.e., starting and ending with the same state $S_a = S_z$. The corresponding NACTs are $\tau_k^{a,b}$, $\tau_k^{b,c}$, ... , $\tau_k^{y,z} = \tau_k^{y,a}$. Let us now consider the product

$$\tilde{\tau}_k^{a,b,c,...,y,z=a} = \tau_k^{a,b}\tau_k^{b,c} \ldots \tau_k^{y,z=a} \quad (16)$$

The IREP of $\tilde{\tau}_k^{a,b,c,...,y,z=a}$ can then be determined from the product theorem for the IREPs of the underlying electronic wave functions $\psi_i(s_e; s)$ and $\psi_j(s_e; s)$ as well as the derivatives of the symmetry-adapted coordinates $\partial/\partial s_k$. Using eq 11 and focusing on 1-d IREPs, we obtain

$$\begin{aligned} \Gamma(\tilde{\tau}_k^{a,b,c,...,y,z=a}) &= \Gamma(\psi_a(s_e;s))^2 \times \Gamma(\psi_b(s_e;s))^2 \times \ldots \times \Gamma(\psi_y(s_e;s))^2 \times \Gamma\left(\frac{\partial}{\partial s_k}\right)^{N_{loop}} \\ &= \begin{cases} \Gamma\left(\frac{\partial}{\partial s_k}\right) & \text{if } N_{loop} \text{ is odd} \\ A_1 & \text{if } N_{loop} \text{ is even} \end{cases} \end{aligned} \quad (17)$$

Theorem 17 imposes a condition on the IREPs of the NACTs $\tau_k^{i,j}$ which contribute to the loop (16). Analogous conditions can be derived for similar loops for NACTs $\tau_k^{a,b}\tau_l^{b,c}$ ... with respect to different symmetry-adapted coordinates s_k, s_l, etc., but these do not provide any additional information because they can be re-expressed in terms of theorems 15 and 17.

In order to demonstrate the power of theorem 17, let us consider the example of C_5H_4NH and the loop of $N_{loop} = 3$ electronic states S_0, S_1, S_2, S_0, thus

$$\tilde{\tau}_k^{0,1,2,0} = \tau_k^{0,1}\tau_k^{1,2}\tau_k^{2,0} \quad (18)$$

For $s_k = \varphi$, theorem 17 yields the relation of the IREPs of the NACTs with respect to the $\partial/\partial\varphi$ derivatives

$$\Gamma(\tilde{\tau}_\varphi^{0,1,2,0}) = \Gamma(\tau_\varphi^{0,1}) \times \Gamma(\tau_\varphi^{1,2}) \times \Gamma(\tau_\varphi^{2,0}) = \Gamma\left(\frac{\partial}{\partial\varphi}\right) = A_2 \quad (19)$$

Likewise, for the NACTs with respect to the $\partial/\partial r$ derivatives, theorem 17 yields

$$\Gamma(\tilde{\tau}_r^{0,1,2,0}) = \Gamma(\tau_r^{0,1}) \times \Gamma(\tau_r^{1,2}) \times \Gamma(\tau_r^{2,0}) = \Gamma\left(\frac{\partial}{\partial r}\right) = A_1 \quad (20)$$

The relations 19 and 20 for the NACTs with respect to the derivatives $\partial/\partial\varphi$ and $\partial/\partial r$, respectively, imply symmetry constraints on their IREPs. For example, if the IREPs are known for two of the NACTs with respect to $\partial/\partial\varphi$, say, $\Gamma(\tau_\varphi^{0,1})$ and $\Gamma(\tau_\varphi^{0,2})$, then the IREP of the third one, i.e., $\Gamma(\tau_\varphi^{1,2})$, follows automatically from relation 19. An example is anticipated in Table 1, i.e., $\Gamma(\tau_\varphi^{0,1}) = \Gamma(\tau_\varphi^{0,2}) = B_1$ implies $\Gamma(\tau_\varphi^{1,2}) = A_2$. Note that, on one hand, theorem 17 establishes a useful relation (or more, if additional loops of electronic states are available) between the NACTs of the loop of electronic states (16). On the other hand, it does not suffice per se to discover the IREPs of all of the NACTs; additional steps are necessary, for that purpose; see item vi. In any case, the two theorems 15 and 17 are applicable without ever calculating the electronic wave functions or the NACTs explicitly.

F. Signs of NACTs at Symmetry-Related Positions. (vi) Next, we note that theorem 15 allows one to determine relations between different patterns of relative signs of the NACTs at the sets of symmetry-related values of coordinates, as well as corresponding different symmetric nodes for the $\tau_k^{i,j}(s)$, depending on the IREPs of the different derivatives $\partial/\partial s_k$. For this

purpose, let us assume that the IREP of $\tau_k^{i,j}(s)$ is $\Gamma(\tau_k^{i,j}(s)) = \Gamma_g$, and the value of $\tau_k^{i,j}(s)$ at a reference location $s = [\{s_l\}]_1$ has been determined to be $\tau_k^{i,j}([\{s_l\}]_1)$. Then, one can apply the symmetry projection operator $\hat{P}^{\Gamma_g}$ to generate the values of $\tau_k^{i,j}([\{s_l\}]_h)$ at all of the symmetry-related locations $[\{s_l\}]_h$. Their absolute values are identical, cf. eq 12, but the patterns of the relative signs may differ, depending on the characters $\chi_{g,h}$ which are involved in $\hat{P}^{\Gamma_g}$; see eq 2. Whenever the signs of $\tau_k^{i,j}([\{s_l\}_f])$ and $\tau_k^{i,j}([\{s_l\}]_h)$ are different, there must be a node of $\tau_k^{i,j}(s)$ located halfway between $[\{s_l\}_f]$ and $[\{s_l\}]_h$, i.e.,

$$\tau_k^{i,j}(s_{fh}) = 0 \quad \text{at} \quad s_{fh} = \frac{1}{2}([\{s_l\}]_f + [\{s_l\}]_h) \tag{21}$$

if

$$\tau_k^{i,j}([\{s_l\}]_f) = -\tau_k^{i,j}([\{s_l\}]_h)$$

for the given IREP, $\Gamma(\tau_k^{i,j}(s)) = \Gamma_g$. Now theorem 15 implies that the IREPs of $\tau_k^{i,j}(s)$ and $\tau_l^{i,j}(s)$ differ if $\Gamma(\partial/\partial s_k) \neq \Gamma(\partial/\partial s_l)$. By analogy of the derivation of eq 21, the patterns of the relative signs of the NACTs $\tau_k^{i,j}([\{s_l\}]_g)$ and $\tau_l^{i,j}([\{s_l\}]_g)$ at symmetry-related coordinates $[\{s_l\}]_g$, as well as the corresponding nodes (21) should also differ, according to their IREPs.

For the present example C_5H_4NH with molecular symmetry group $C_{2v}(M)$, Table 1 lists schemes of the different patterns of signs of the NACTs, as well as the different nodes, depending on their IREPs, for all four possibilities which are in accordance with theorem 15. For example, consider the third possibility when $\Gamma(\tau_x^{i,j}) = A_1$. The corresponding sign pattern implies that the $\tau_x^{i,j}(\hat{S}_g[\{r, \varphi\}])$ at all symmetry-related values of coordinates $\hat{S}_g[\{r, \varphi\}]$, eq 7, have the same sign. Hence, $\tau_x^{i,j}(s)$ does not possess any symmetry nodes. In contrast, $\Gamma(\tau_y^{i,j}) = A_2$; hence, $\tau_y^{i,j}(\hat{S}_g[\{r, \varphi\}])$ has a pattern of alternating signs at the symmetry-related coordinates $\hat{S}_g[\{r, \varphi\}]$, and both the x- and y-axes are nodal lines. Likewise, $\tau_\varphi^{i,j}$ and $\tau_r^{i,j}$ have the IREPs B_1 and B_2, with corresponding different patterns of the relative signs, and also with different x- or y-axes as nodal lines, respectively, as illustrated schematically in Table 1. Note that these nodal lines are infinite; i.e., they will impose corresponding changes of the sign of the values of the NACTs even far away from any conical intersections: this will be exploited for the subsequent quantum chemistry calculations of the NACTs, cf. item xi.

G. Determination of the Irreducible Representations (IREPs) of the NACTs. (vii) The results of steps i−vi, in particular, the two general theorems 15 and 17 together with the consequences for the patterns of the relative signs and nodes of the NACTs, are quite useful, but they do not always suffice to carry out the next task, i.e., to assign the IREPs of the NACTs. For this purpose, we may have to add additional information about the NACTs. In general, the amount of information that is required in order to specify the IREP depends on the size G of the molecular symmetry group. All groups which are isomorphic to molecular point groups can be constructed by means of a maximum of three symmetry operations $\hat{S}_h$ which serve as generators. Accordingly, it suffices to specify no more than three (nontrivial, i.e., beyond $\chi_{g,E} = 1$ for the identity E) characters $\chi_{g,h}$ of these generators, in order to deduce the corresponding IREP Γ_g.[8] Accordingly, three items of information, or even less depending on the size of the MS group, should be sufficient to specify the requested IREP of the NACT. The two general theorems 15 and 17 may be applicable for this purpose. Here, we summarize two additional, well-known[1,2] properties of the NACTs between two succesive isolated states ψ_i, ψ_{i+1}, related to the CIs, and another property which involves a third electronic state, cf. items a, b, and c below. These will provide complementary information for the task of assigning IREPs to NACTs.

(a) The contour integrals[30] over the $\tau^{i,i+1}(s|L_g)$ evaluated along closed loops denoted by L_g around the individual $CI_g^{i,i+1}$ satisfy a quantization rule;[1] i.e., they are equal to $+\pi$ or $-\pi$, depending on the IREP-adapted signs of the $\tau^{i,i+1}$ close to $s_{i,i+1}$

$$\oint \mathrm{d}s \cdot \tau^{i,i+1}(s|L_g) = \pm\pi = e_g^{i,i+1}\pi \tag{22}$$

if the loop L_g encloses one single $CI_g^{i,i+1}$. Here, $e_g^{i,i+1} = \pm 1$ denotes the "charge" of the $CI_g^{i,i+1}$. Else,

$$\oint \mathrm{d}s \cdot \tau^{i,i+1}(s|L_g) = 0 \tag{23}$$

if the loop does not enclose any CI. Here, the dot represents a scalar product of the vectorial NACTs $\tau^{i,i+1}(s|L_g)$ and $\mathrm{d}s$, which have components $\tau_k^{i,i+1}(s|L_g)$ and $\mathrm{d}s_k$ with respect to the symmetry-adapted coordinates s_k, respectively; i.e., the integrations (22) and (33) are over the tangential components of $\tau^{i,i+1}$. For convenience, we shall construct the loops L_g of the contour integrals as a closed sequence of lines along individual symmetry-adapted coordinates.

The quantization rule (22) holds if the loop is sufficiently close to the $CI^{i,i+1}(s^{i,i+1})$ such that NACTs due to other states $j \neq i$, $i + 1$ do not interfere significantly; this corresponds to a two-state $(i, i + 1)$ model.[1] Else, interfering NACTs give rise to more general quantization rules.[1,28] The quantization rule for the NACTs has been exploited previously[15] in order to reveal a conical intersection in a given region of configuration space.[1] In section III, we shall apply an alternative search for conical intersections, based on the above-mentioned Longuet-Higgins phase change theorem, with application to paths in configuration space which may well include large amplitude motions, from reactants via transition states to products, in the electronic ground state.[35,36] So far, these approaches have been used without considerations of the molecular symmetry groups of the NACTs.

(b) The planar $\tau_k^{i,i+1}(s)$ element is assumed to have poles. By this, it is meant that, if it is written as $\tau_k^{i,i+1}(\tilde{r}, \tilde{\varphi})$, where $(\tilde{r}, \tilde{\varphi})$ are polar coordinates for an origin at the given conical intersection point, it becomes singular at $\tilde{r} = 0$ and decays to zero like $1/\tilde{r}$ as $\tilde{r} \to \infty$,[1] with the $\pm$ signs imposed by the IREPs

$$\tau_k^{i,i+1}(s) \to \pm\infty \quad \text{for} \quad s \to (s^{i,i+1}) \tag{24}$$

(c) The wave function $\psi_j(s_e; s)$ and $\psi_{j+1}(s_e; s)$ may change characters as the nuclear coordinates s pass from one side, say, the "left, s_l" hand side across the seam of $CI^{j,j+1}(s^{j,j+1})$ to the other one, say, the "right, s_r" hand side. For example, if $\psi_j(s_e; s_l)$ and $\psi_{j+1}(s_e; s_r)$ represent essentially covalent or diradical types of bonding, then these characters may switch to $\psi_{j+1}(s_e; s_r)$ and $\psi_j(s_e; s_l)$, respectively. If this switch occurs close to a specific configuration of the seam, say, at $[s^{j,j+1}]_1$, then molecular symmetry implies that equivalent switches occur at all other symmetry-adapted locations $[s^{j,j+1}]_g$. As a consequence, the wave functions ψ_j and ψ_{j+1} have the same IREPs. The definition (11) then implies that the NACTs $\tau_k^{i,j}(s)$ and $\tau_k^{i,j+1}(s)$ between two different states $i < j$ and $j + 1$ should also

interchange. Moreover, relation 11 yields the same IREPs for the NACTs $\tau_k^{i,j}(s)$ and $\tau_k^{i,j+1}$. Turning the table,

$$\Gamma(\tau_k^{i,j}) = \Gamma(\tau_k^{i,j+1}) \tag{25}$$

in case of a switch

$$\tau_k^{i,j}(s_l) \rightarrow \tau_k^{i,j+1}(s_r) \tag{26}$$

$$\tau_k^{i,j+1}(s_l) \rightarrow \tau_k^{i,j}(s_r) \tag{27}$$

close to $CI^{j,j+1}(s^{j,j+1})$.

For the present model system C_5H_4NH, the size of the molecular symmetry group $C_{2v}(M)$ is just $G = 4$; i.e., in order to assign the IREPs Γ_g of the NACTs (and consequently the corresponding CIs, cf. item ix), one has to determine just two nontrivial characters $\chi_{g,h}$. For this purpose, one has to provide just two pertinent pieces of information. As an example, we shall consider the cases where a conical intersection $CI^{i,i+1}(s^{i,i+1})$ has been discovered at specific values of the symmetry-adapted coordinates $[s^{i,i+1}]_1 = [\{r^{i,i+1}, \varphi^{i,i+1} = \pi/2\}]_1$. We shall then employ the two properties (22) and (24) of these CIs in order to determine the IREPs of the associated $\tau_k^{i,i+1}(s)$. The derivation is given in the next paragraphs, using theorem 15 and the corresponding relations of the patterns of the relative signs and nodes of the NACTs; see Table 1. Later on, we shall apply the result to the special case of $\tau_k^{0,1}(s)$, cf. step xi. Subsequently, we shall use the rule (25) in order to determine the same IREPs of the NACTs $\tau_k^{0,1}(s)$ and $\tau_k^{0,2}(s)$. Finally, we shall apply theorem 17 in order to determine the IREPs of the NACTs which are still missing, i.e., $\tau_k^{1,2}(s)$.

The task of assigning the IREPs to all of the NACTs $\tau_k^{i,i+1}(\varphi,r)$ can be reduced to another one, i.e., determining the appropriate combination of IREPs of the NACTs, out of four possibilities which are listed in Table 1; this reduction is a consequence of theorem 17. For this purpose, we will first employ the quantization rule (22) for $CI^{i,i+1}(\{r^{i,i+1}, \varphi^{i,i+1} = \pi/2\})$, as specified in eq 28 below, in order to eliminate two of the four possible combinations of IREPs of the NACTs which are listed in Table 1. Subsequently, we shall apply the pole property (24) in order to eliminate another possibility, thus determining the one and only one combination of the IREPs of the NACTs which is left after elimination of the other three choices.

The example where a conical intersection $CI_1^{i,i+1}([s^{i,i+1}]_1)$ has been discovered at $[s^{i,i+1}]_1 = [\{r^{i,i+1}, \varphi^{i,i+1} = \pi/2\}]_1$ is illustrated schematically in Figure 2a. In order to apply the quantization rule (22), we construct the loop L_1 around $CI_1^{i,i+1}(s^{i,i+1})$ in the (r, φ)-plane, as shown in Figure 2a, cf. figure legend. The contour integral (22) then consists of three contributions for the torsional (tor) and two radial (rad) lines of the loop

$$\oint \mathrm{d}s \cdot \tau^{i,i+1}(s|L_1) = I_{\mathrm{tor}} + I_{\mathrm{rad},1} + I_{\mathrm{rad},2} = e_1^{i,i+1}\pi \tag{28}$$

where

$$I_{\mathrm{tor}} = \int_{\varphi_2}^{\pi-\varphi_2} \mathrm{d}\varphi \tau_\varphi^{i,i+1}(r_1, \varphi|L_1) \tag{29}$$

$$I_{\mathrm{rad},1} = \int_0^{r_1} \mathrm{d}r \tau_r^{i,i+1}(r, \varphi_2|L_1) \tag{30}$$

$$I_{\mathrm{rad},2} = \int_{r_1}^{0} \mathrm{d}r \tau_r^{i,i+1}(r, \pi - \varphi_2|L_1) \tag{31}$$

Its absolute value should be equal to π;[1] the sign or "charge" $e_1^{i,i+1}$ is arbitrary because the signs of the underlying wave functions ψ_i and ψ_{i+1} are arbitrary, cf. eq 10. The choice $e_1^{i,i+1} = +1$ in eq 28 is made ad hoc, for convenience of the subsequent illustrations, see section III; it implies corresponding consistent sets of relative (same or opposite) signs or charges of all the NACTs and CIs, but it will not affect any of the subsequent conclusions. Accordingly, we assign the charge $e_1^{i,i+1} = 1$ to $CI^{i,i+1}([\{r^{i,i+1}, \varphi^{i,i+1} = \pi/2)\}]_1)$, as shown in Figure 2a. The specification (28) of the quantization rule (22) will now allow us to eliminate the second and fourth combinations of the IREPs of the NACTs which have been

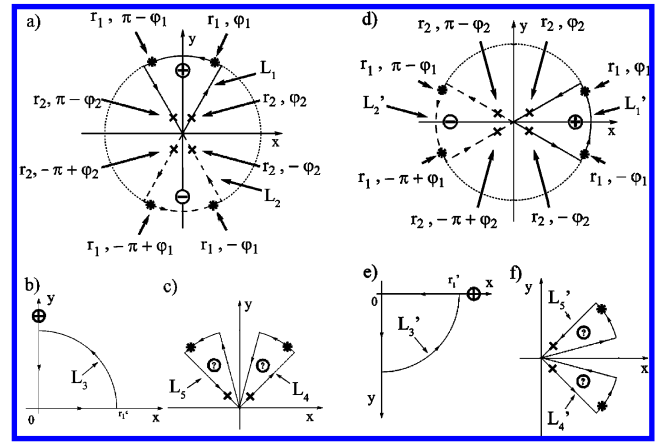

Figure 2. Determination of the IREPs of the NACTs $\tau_k^{i,i+1}(s)$ and the corresponding IREPs and seams of the CIs, for two cases where a conical intersection $CI_1^{i,i+1}$ has been discovered at the symmetry-adapted coordinates $[s^{i,i+1}]_1 = [\{r^{i,i+1},\varphi^{i,i+1}\}]_1$, where $\varphi^{i,i+1} = \pi/2$ (panels a−c) or 0 (panels d−f); see also Figure 1. The CIs are surrounded by loops L_1 (L_1') which are drawn by continuous lines. They consist of three parts, as indicated by three small arrows: a "torsional" line along the torsional angle φ, from $\varphi = \varphi_2$ to $\pi - \varphi_2$ (panel a) or from $\varphi = -\varphi_2$ to $+\varphi_2$ (panel d), and two "radial" lines with opposite directions along the radial coordinate r, from 0 to r_1 and from r_1 to 0, respectively. The values of the contour integrals (22) for these loops are assumed to be π; the + sign is used as "charge" $e_1^{i,i+1} = 1$ for these CIs. The symmetry properties of the NACTs are derived from their values at symmetry-related locations on the loops, which are indicated by asterisks (*) on the torsional line and by crosses (×) on the radial lines. Bold arrows point to these symbols * and ×, indicating their symmetry-related values of the coordinates, cf. Table 1. The irreducible representations of the NACTs and CIs imply the existence of additional symmetry-related $CI_2^{i,i+1}$ which have opposite charges, $e_2^{i,i+1}$. These are surrounded by equivalent loops L_2 (L_2') (dashed lines) with additional symmetry-related positions which are labeled again by the symbols * and ×, respectively. The NACTs at these locations * and × on the dashed loops L_2 (L_2') have the same absolute values as for the continuous loops L_1 (L_1') but opposite signs. Panels b and e show loops L_3 and L_3' which do not encircle these CIs; they consist of three parts, i.e., a quarter circle along the torsional angle φ which approaches the CIs located at $\varphi^{i,i+1} = \pi/2$ (panel c) or 0 (panel d), plus two lines along the x and y axes. The contour integrals (23) for these loops L_3 (L_3') are zero. Finally, panels c and f with the loops L_4, L_5 (L_4', L_5') around two hypothetical symmetry-related $CI^{i,i+1}(s^{i,i+1})$ (indicated by ?) are used to show that the seams of the conical intersections are restricted to symmetry-adapted coordinates $s^{i,i+1} = \{r^{i,i+1},\varphi^{i,i+1}\}$, where $\varphi_{i,i+1} = \pi/2$ and $-\pi/2$ or 0 and $-\pi$ or $+\pi$, respectively; see text.

specified in Table 1: both have alternating relative signs of $\tau_{\varphi}^{i,i+1}(r_1, \varphi)$ at the symmetry-related coordinates (e.g., see the stars on loop L_1 in Figure 2a) which contribute to the torsional integral (29), hence $I_{\text{tor}} = 0$. Moreover, the NACTs $\tau_r^{i,i+1}(r, \varphi_2|L_1)$ and $\tau_r^{i,i+1}(r, \pi - \varphi_2|L_1)$ which contribute to the radial integrals (30) and (31), respectively, are identical (e.g., see the crosses × on loop L_1 in Figure 1a) so that $I_{\text{rad},1} + I_{\text{rad},2} = 0$. As a consequence, the second and fourth combinations of IREPs would yield $I_{\text{tor}} + I_{\text{rad},1} + I_{\text{rad},2} = 0$, which is incompatible with the quantization rule (28) for the NACTs. For the time being, we are thus left with just two possible combinations of IREPs of the NACTs, i.e., either the first or the third one, cf. Table 1.

Next, we shall exploit the pole property of the NACTs close to $\text{CI}^{i,i+1}$, i.e., rule 24, in order to eliminate the first combination of IREPs of the NACTs, cf. Table 1. For this purpose, let us consider loop L_3 which is shown in Figure 2b: it consists of a quarter circle (quc) and two lines along the y- and x-axes. The radius r' of the quarter circle is chosen such that the loop does not encircle the CI but it approaches the CI for $\varphi \rightarrow \pi/2$, implying ever increasing absolute values of $\tau_{\varphi}^{i,i+1}(r',\varphi)$, cf. rule 24. According to eq 23, the corresponding contour integral should be equal to zero. We shall show that this requirement cannot be satisfied by the first possible combination of IREPs of the NACTs, cf. Table 1. Again, the contour integral may be separated into three line integrals, specifically for the quarter circle (quc) plus the contributions on the y- and x axes,

$$\oint \mathrm{d}s \cdot \tau^{i,i+1}(s|L_3) = I_{\text{quc}} + I_y + I_x = 0 \qquad (32)$$

where

$$I_{\text{quc}} = \int_0^{\pi/2} \mathrm{d}\varphi \tau_{\varphi}^{i,i+1}(r', \varphi|L_3) \qquad (33)$$

$$I_y = \int_{r'}^{0} \mathrm{d}y \tau_y^{i,i+1}(x = 0, y|L_3) \qquad (34)$$

$$I_x = \int_0^{r'} \mathrm{d}x \tau_x^{i,i+1}(x, y = 0|L_3) \qquad (35)$$

Now for the first possible combination of IREPs of the NACTs, on one hand, $\tau_x^{i,i+1}$ and $\tau_y^{i,i+1}$ have nodes along the x- and y-axes; hence, $I_x = I_y = 0$, cf. Table 1. On the other hand, rule 24 implies that $I_{\text{quc}} \neq 0$ because it is dominated by the large contributions of $\tau_{\varphi}^{i,i+1}(r',\varphi|L_3)$ close to $\varphi = \pi/2$. The net result is thus $I_{\text{quc}} + I_x + I_y \neq 0$, which is incompatible with eq 32.

In conclusion, if a conical intersection $\text{CI}_1^{i,i+1}$ is discovered at $\varphi^{i,i+1} = \pi/2$, then the quantization of the NACTs, eq 22, together with the pole property of the NACTs close to the CI, eq 24, eliminate all possible combinations of the IREPs of the NACTs, except the third one; thus, $\Gamma(\tau_{\varphi}^{i,i+1}(s)) = B_1$, $\Gamma(\tau_r^{i,i+1}(s)) = B_2$, etc., cf. Table 1. This result is a global property, i.e., independent of the coordinates which are used in the derivation. It is equivalent to say that the two properties (22) and (24) of $\text{CI}_1^{i,i+1}$, together with theorem 15, determine the IREPs $\Gamma(\tau_k^{i,i+1}(s))$ of all of the NACTs, and this is equivalent to determining two nontrivial characters $\chi_{g,h}$ for each of them.

Likewise, let us consider another example where $\text{CI}_1^{i,i+1}$ is discovered at $\varphi^{i,i+1} = 0$. Arguments which are entirely analogous to those which have just been applied to $\text{CI}^{i,i+1}([\{r^{i,i+1}, \varphi^{i,i+1} = \pi/2\}]_1)$ allow one to eliminate all possible combinations of IREPs of the NACTs, except the fourth one, cf. Table 1. The loops L_1' and L_3' for the corresponding contour integrals are shown in Figure 2d and e, analogous to those shown in panels a and b, respectively. In particular, the quantization of the NACTs (22) applied to the contour integral for the loop L_1' shown in Figure 2d eliminates the second and third combinations of the IREPs of the NACTs, whereas rule 24 for the pole property of the NACTs close to $\text{CI}_1^{i,i+1}$ applied to the contour integral for loop L_3' shown in Figure 2e eliminates the first combination.

H. Charges of the Conical Intersections at Symmetry-Related Positions. (viii) After determination of the IREPs of the NACTs $\tau_k^{i,i+1}(s)$, it is straightforward to define the corresponding charges of the $\text{CI}_g^{i,i+1}$ at all symmetry-related coordinates $[\{r^{i,i+1}, \varphi^{i,i+1}\}]_g$, $g = 1, 2, 3, 4$. For the first example where $\text{CI}_1^{i,i+1}$ has been located at $[\{r^{i,i+1}, \varphi^{i,i+1} = \pi/2\}]_1$, applications of the symmetry operations $\hat{S}_1 = E$ and $\hat{S}_4 = (12)^*$ yield the same locations $[\{r^{i,i+1}, \varphi^{i,i+1}\}]_1 = [\{r^{i,i+1}, \varphi^{i,i+1}\}]_4$, whereas the operations $\hat{S}_2 = (12)$ and $\hat{S}_3 = E^*$ yield the "opposite" location $[\{r^{i,i+1}, \varphi^{i,i+1}\}]_2 = [\{r^{i,i+1}, \varphi^{i,i+1}\}]_3 = \{r^{i,i+1}, -\pi/2\}$. For this case, the complete set of symmetry-related CIs consists, therefore, of just two species, $\text{CI}_1^{i,i+1} = \text{CI}^{i,i+1}([\{r^{i,i+1}, \varphi^{i,i+1} = \pi/2\}]_1)$ and $\text{CI}_2^{i,i+1} = \text{CI}^{i,i+1}([\{r^{i,i+1}, \varphi^{i,i+1} = -\pi/2\}]_2)$. We shall now show that these two CIs have opposite charges, as illustrated in Figure 2a. For this purpose, we use $\hat{S}_2 = (12)$ to map loop L_1 around $\text{CI}_1^{i,i+1}$ (continuous lines) on the symmetry-related loop L_2 around $\text{CI}_1^{i,i+1}$ (dashed lines), cf. Figure 2a. Corresponding symmetry-related locations on the torsional and radial lines are marked again by stars and crosses, respectively. The IREP $\Gamma(\tau_{\varphi}^{i,i+1}) = B_1$ implies that the NACTs $\tau_{\varphi}^{i,i+1}(s|L_1)$ and $\tau_{\varphi}^{i,i+1}(s|L_2)$ at the locations "*" on the torsional paths of loops L_1 and L_2 have the same absolute values but opposite signs, cf. Table 1. Likewise, the IREP $\Gamma(\tau_r^{i,i+1}) = B_2$ implies that the NACTs $\tau_r^{i,i+1}(s|L_1)$ and $\tau_r^{i,i+1}(s|L_2)$ at the locations "×" on opposite radial segments of loops L_1 and L_2 also have the same absolute values but opposite signs. As a consequence, if the contour integral (28) for loop L_1 is equal to $+\pi$, then the analogous contour integral for loop L_2 has the opposite value, $-\pi$. These opposite signs are then used to assign opposite charges $e_1^{i,i+1} = +1$ and $e_2^{i,i+1} = -1$ to $\text{CI}_1^{i,i+1}$ or $\text{CI}_2^{i,i+1}$, respectively. Analogous arguments may be applied to the second example where the CI has been located at $[\{r^{i,i+1}, \varphi^{i,i+1} = 0\}]_1$. Again, applications of all symmetry operations $\hat{S}_k$ yield the complete set of symmetry-related CIs which consists of just two species, $\text{CI}_1^{i,i+1} = \text{CI}^{i,i+1}([\{r^{i,i+1}, \varphi^{i,i+1} = 0\}]_1)$ and $\text{CI}_2^{i,i+1} = \text{CI}^{i,i+1}([\{r^{i,i+1}, \varphi^{i,i+1} = \pm\pi\}]_2)$. Application of $\hat{S}_2 = (12)$ maps loop L_1' around $\text{CI}_1^{i,i+1}$ to loop L_2' around $\text{CI}_2^{i,i+1}$, cf. Figure 2d. The IREPs $\Gamma(\tau_{\varphi}^{i,i+1}) = B_2$ and $\Gamma(\tau_r^{i,i+1}) = B_1$ imply opposite values $+\pi$ and $-\pi$ of the contour integrals for loop L_1' and L_2', imposing opposite charges $e_1^{i,i+1} = +1$ and $e_2^{i,i+1} = -1$ on $\text{CI}_1^{i,i+1}$ and $\text{CI}_2^{i,i+1}$, respectively, cf. Figure 2d. The derivation of the opposite charges of the conical intersections for the second example in terms of Cartesian coordinates is shown in Appendix A.

In the subsequent applications, we shall also encounter the case where a conical intersection $\text{CI}^{j,j+1}([\{r^{j,j+1}, \varphi^{j,j+1}\}]_1)$ is discovered for another set of PESs labeled V_j and V_{j+1}, at values $\varphi^{j,j+1}$ different from 0, $+\pi/2$, $-\pi/2$, or $\pm\pi$. Again, we shall employ the properties of the CIs in order to determine the IREPs of the corresponding NACTs $\tau_k^{j,j+1}(r,\varphi)$, but the task will be facilitated by the fact that we already know the IREPs of $\tau_k^{i,i+1}(r, \varphi)$ which have been determined for $\text{CI}^{i,i+1}([\{r^{i,i+1}, \varphi^{i,i+1}\}]_1)$ for the PESs V_i and V_{i+1} located at $\varphi^{i,i+1} = \pi/2$ or 0, cf. Figure 2a and d, respectively.

I. Irreducible Representations of the Conical Intersections. (ix) After the assignment of the charges of the $\text{CI}_g^{i,i+1}$ at all of the symmetry-related locations $[s]_g$ with $g = 1, \ldots, G$ (see item viii), one may apply the projection operators (2) to

the set of charged $CI^{i,i+1}$ in its order to assign its IREP. In brief,

$$\Gamma(CI^{i,i+1}) = \Gamma_h \tag{36}$$

if

$$\hat{P}^{\Gamma_h} CI^{i,i+1} = CI^{i,i+1} \tag{37}$$

Application to our model system C_5H_4NH with MS group $C_{2v}(M)$ yields

$$\Gamma(CI^{i,i+1}) = B_1 \quad \text{if} \quad \varphi^{i,i+1} = \pi/2 \tag{38}$$

and

$$\Gamma(CI^{i,i+1}) = B_2 \quad \text{if} \quad \varphi^{i,i+1} = 0 \tag{39}$$

where $\varphi^{i,i+1}$ denotes the "first" conical intersection; see also the relative signs which are listed for arbitrary objects with irreducible representations B_1 and B_2 in Table 1, respectively.

J. Molecular Symmetry Effects on the Topology of Conical Intersections. (x) Finally, we discover an important consequence of items i−ix; i.e., the domains of the seams of the CIs may be restricted to specific topologies due to molecular symmetry. As an example, consider the case where $CI_1^{i,i+1}$ has been discovered at $[\{r^{i,i+1}, \varphi^{i,i+1} = \pi/2\}]_1$, implying the symmetry-adapted $CI_2^{i,i+1}$ at $[\{r^{i,i+1}, \varphi^{i,i+1} = -\pi/2\}]_2$, cf. Figure 2a. We shall show that, for this scenario, the seam of the CIs in the (r, φ)-plane are constrained to $\varphi^{i,i+1} = \pm\pi/2$. For this purpose, let us assume hypothetically that the seam of this conical intersection with symmetry B_1 (cf. item ix) includes a CI which is not located at $\varphi = \pi/2$ or $\varphi = -\pi/2$, as illustrated by one of the hypothetical marks "?" in Figure 2c; application of all symmetry operations would then generate the set of analogous CIs at symmetry-related locations; two representatives of these kinds of hypothetical CIs are illustrated by marks "?" in Figure 2c, with corresponding coordinates $\{s_k^{i,i+1}\}$ which include the values $\varphi^{i,i+1}$ and $\pi - \varphi^{i,i+1}$, respectively, $0 \le \varphi^{i,i+1} < \pi/2$. Figure 2c also shows symmetry-related contours L_4 and L_5 around these hypothetical CIs; they contain the same symbols * and × as those shown in Figure 2a. The symmetries of the NACTs which have been determined in item vii yield the same values (= $+\pi$) of the contour integrals evaluated along these contours. Now let us walk from each of the hypothetical CIs which have been sketched in Figure 2c along the hypothetical seam to the original CI which has been marked by "+" in Figure 2a. Simultaneously, the two loops L_4 and L_5 around the two individual hypothetical CIs are merged to a single one which contains two hypothetical CIs. The contour integral along the single loop is then equal to the sum of the individual loop integrals; i.e., it is equal to $+2\pi$. On arrival at the original $CI_1^{i,i+1}$, let the merged loop coincide with the one shown in Figure 2a. However, we know from item viii that the loop integral for that single loop is equal to $+\pi$, not $+2\pi$, cf. eq 28. This contradiction falsifies the assumption of the hypothetical CIs. The seams of the $CI_1^{i,i+1}$ and $CI_2^{i,i+1}$ are restricted, therefore, to $\varphi^{i,i+1} = \pi/2$ or $-\pi/2$.

Analogous arguments can be applied to the other example where $CI_1^{i,i+1}$ has been discovered at $\varphi^{i,i+1} = 0$, with the symmetry-adapted $CI_2^{i,i+1}$ at $\pm\pi$, cf. Figure 2d. Their seams in the (r, φ)-plane are restricted by molecular symmetry to the values $\varphi^{i,i+1} = 0$ or $\pm\pi$. Assumptions of hypothetical CIs on the seam at different symmetry-related coordinates $\varphi^{i,i+1}$ and $-\varphi^{i,i+1}$ where $0 \le \varphi^{i,i+1} < \pi/2$ surrounded by loop L_4' and L_5', as shown in panel 2f, would lead to contradictions, analogous to the preceding paragraph. By extrapolation, these two examples show that for specific planes of the MS-adapted coordinates, the seams of the CIs may be restricted to specific values of some of the symmetry-adapted coordinates, depending on the symmetry of the NACTs and CIs.

III. Application and Discussions Based on Quantum Chemistry Results for the Model System C_5H_4NH

Section II contains the rather general recipe of steps i−x for the determination of the IREPs of the NACTs and CIs, for molecules with molecular symmetry group supporting 1-d IREPs. The model system C_5H_4NH has served as an example; so far, we have exploited the rather general properties of the corresponding molecular symmetry group $C_{2v}(M)$. In this section, we shall add quantum chemistry *ab initio* evaluations of the NACTs in restricted domains, in order to determine the IREPs of the NACTs and CIs for the lowest three singlet states, and to explore the topologies of the seams of the CIs. For a coherent presentation of the results, we shall refer to the previous items i−x, adding the new ones xi and xii.

(i) The molecular symmetry group of C_5H_4NH is $C_{2v}(M)$, cf. section II.

(ii and iii) It is convenient to solve these combined tasks step by step, as follows:

Step 1: The location of the first $CI_1^{0,1}$ between electronic states S_0 and S_1 is based on the Longuet-Higgins theorem.[32,33] In practice, it involves several substeps:[39]

First, we employ quantum chemistry to calculate the potential minima and transition states (TS) for the PES of the electronic ground state S_0. All of the results presented below (also those for the other PES, the NACTs, the double and triple CIs, and the seams of the CIs) have been obtained at the CAS(10/9)/cc-pVDZ level of the CASSCF methodology[40] as implemented in the GAMESS[41] and MOLPRO[42] program suites. The active space of the CASSCF calculations includes 9 molecular orbitals (MO) occupied by 10 electrons, i.e., all π orbitals (three occupied π ones and three unoccupied π^* orbitals), together with three σ-type MOs (the occupied one for the lone electronic pair of the N atom, the occupied N−H bond MO, and the virtual σ^* (mainly N−H) MO). These σ-MOs were taken into account because the studied syn−anti isomerization involves a change in hybridization of the N atom; see below. The full π-active space together with these σ orbitals provide an adequate description for this part of the PES, using the standard cc-pVDZ basis set. Different from the rest of this paper, these CASSCF calculations employ the "local" molecular point groups of these stationary states, as is adequate for quantum chemistry. The resulting planar geometry of C_5H_4NH at the potential minimum is shown in Figure 3; it is called the *syn-A′* form of C_5H_4NH, with IREP A' for the local C_s symmetry.

The "global" molecular symmetry $C_{2v}(M)$ implies that C_5H_4NH possesses an equivalent minimum of the PES for the anti form, again with local IREP A'. The two electronic valence bond (VB) structures for the syn and anti geometries, with different orientations of the lone electron pairs due to sp^2 hybridization at the nitrogen, are sketched in Figure 4.

In-plane inversion of the CNH fragment of C_5H_4NH from its syn form to the anti form leads via the transition state for

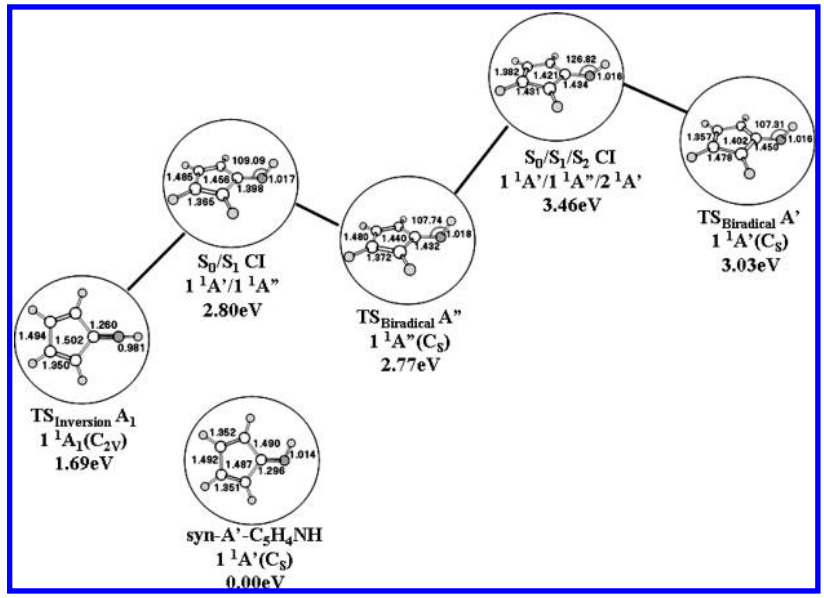

Figure 3. Geometries of the syn form of C_5H_4NH in the electronic ground state S_0, three transition states (TS) between the syn and anti forms, and two conical intersections (CIs) which are located on the paths (continuous lines, schematic) between the TS with opposite local IREPs A' and A''. The results are obtaind by CAS(10/9)/cc-pVDZ calculations. Also shown are the IREPs for the local molecular point groups (NOT the molecular symmetry group!) and the energies relative to the minimum of the adiabatic potential V_0 in the electronic ground state.

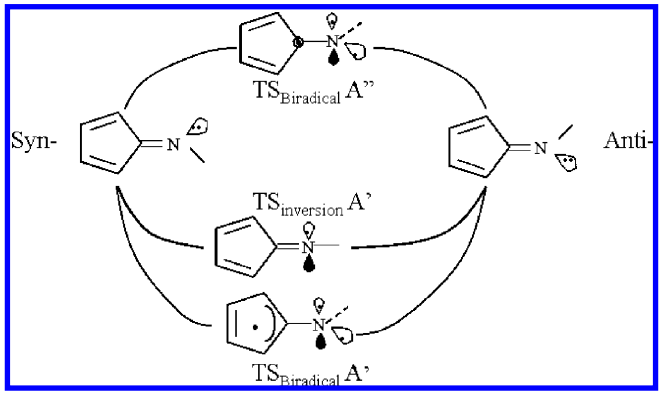

Figure 4. Valence bond (VB) structures of the syn and anti forms of C_5H_4NH in the electronic ground state and three transitions states for syn−anti isomerization, together with three Longuet-Higgins (LH) loops which connect these stationary points or "anchors".

inversion, denoted as $TS_{inversion}$. It is located halfway between the syn and anti configurations, with corresponding IREP A_1 of the local molecular point group C_{2v}, and with energy relative to the syn form as documented in Figure 3. Isomerization via $TS_{inversion}$ does not involve the breaking or making of chemical chemical bonds, but the N atom changes hybridization from sp^2 at the potential minima to sp + p at $TS_{inversion}$, as illustrated schematically in Figure 4. The geometries of the reactant, products, and $TS_{inversion}$ are similar except for the CNH bond angle and the CN and NH bond lengths, which are shorter for $TS_{inversion}$ than for the minima, due to sp hybridization (see Figures 3 and 4).

In contrast with inversion, torsion of the NH bond around the CN axis of the C_5H_4N fragment leads to a biradical structure which supports two different transition states with the same local C_s symmetry but different geometries, energies, electronic VB structures, and local IREPs of the electronic wave function; accordingly, these are denoted $TS_{biradical}$ A' and $TS_{biradical}$ A'', cf. Figures 3 and 4. Specifically, the VB structures of both biradical TSs have one unpaired electron located on a p orbital of the N atom (orthogonal to the π-system), but the other unpaired electron differs; i.e., for the $TS_{biradical}$ A'', it is localized at the C atom of the CN bond, whereas, for $TS_{biradical}$ A', it spreads on the allyl fragment.

Molecular symmetry C_{2v}(M) implies that the symmetry operations (12), E^*, and (12)* would map these three TS to analogous molecular-symmetry-adapted ones, but for the present purpose of localizing the first $CI_1^{0,1}$ between V_0 and V_1, it suffices to know just those species which are illustrated in Figures 3 and 4, together with the corresponding energies, local (!) symmetries and IREPs of the electronic wave function $\psi_0(s_e; s)$. Note that the quantum chemistry results do not provide any direct information about the global IREPs of the molecular symmetry C_{2v}(M).

Second, we construct the so-called Longuet-Higgins (LH) loops. For this purpose, the stationary points, i.e., the minima and transition states of the PES V_0(s) of C_5H_4NH in the electronic ground state S_0 are considered as so-called "anchors".[31] The LH loops connect few selected anchors. Three different LH loops are shown in Figure 4. Each of them consists of a unique pair of reaction paths from the syn form of C_5H_4NH via one of the three different TSs to the anti form.

Third, we determine whether the LH loops are sign preserving, or sign inverting. The criteria are given in ref 39, based on a comparison of the IREPs of the electronic wave function $\psi_0(s_e; s)$ with respect to the same local molecular point group. For this purpose, we note that all of the potential minima and the two $TS_{biradical}$ have local C_s symmetry. For $TS_{inversion}$, let us consider, therefore, the same subgroup C_s of the local molecular point group C_{2v}. The IREP A_1 of $TS_{inversion}$ then correlates with A' for the subgroup C_s of C_{2v}. As a result, the LH loop denoted LH_1 = (*syn*-A' − $TS_{inversion}$ A' − *anti*-A' − $TS_{biradical}$ A' − *syn*-A') is sign preserving, because the electronic wave function has the same local (!) IREPs A' at all of the anchors. In contrast, the two other loops denoted LH_2 = (*syn*-A' − $TS_{inversion}$ A' − *anti*-A' − $TS_{biradical}$ A'' − *syn*-A') and LH_3 = (*syn*-A' − $TS_{biradical}$ A' − *anti*-A' − $TS_{biradical}$ A'' − *syn*-A') are sign inverting because they involve different local IREPs, A' and A''.[39]

Fourth, according to the LH theorem, a single CI exists within any LH loop if the loop contains the minimum number of anchors, and if it is sign inverting. Hence, there are CIs in the

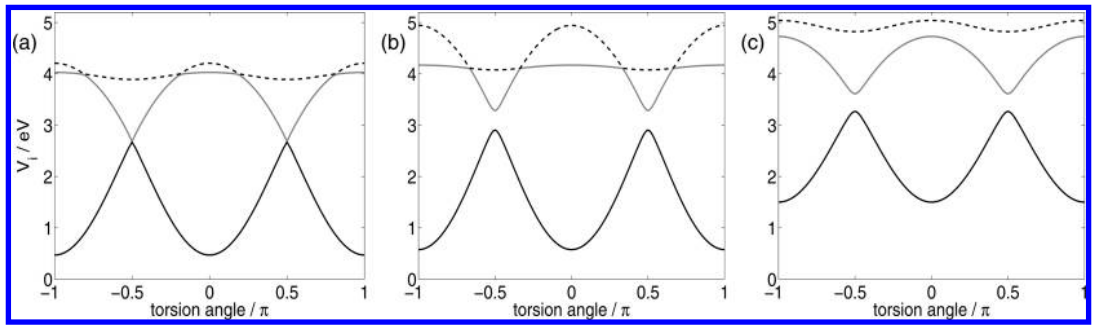

Figure 5. Adiabatic potentials V_0 (black continuous lines), V_1 (gray continuous lines), and V_2 (dashed lines) of C_5H_4NH as a function of the torsional angle φ for $r = 1.0$ Å (a), 0.8 Å (b), and 1.2 Å (c).

LH loops LH_2 and LH_3 but not in LH_1. The CIs can be located by interpolation on paths which connect anchors of the surrounding LH loop with different local IREPs, e.g., between opposite transition states.[39] Specifically, for LH_2, a CI between the PES $V_0(s)$ and $V_1(s)$, denoted as S_0/S_1 CI ($1A'/1A''$), is located on the connecting line between $TS_{inversion}$ $1A'$ and $TS_{biradical}$ $1A''$, close to $TS_{biradical}$ $1A''$. The line is illustrated schematically in Figure 3, together with the geometry and energy of the CI. Likewise, LH_3 should support another CI between V_0 and V_1 located on the line between $TS_{biradical}$ $1A'$ and $TS_{biradical}$ $1A''$. A systematic search along this line yields even a triple degeneracy of V_0, V_1, and in addition V_2. This triple CI is denoted $S_0/S_1/S_2$ CI ($1A'/1A''/2A'$), as shown in Figure 3. A triple CI is a connecting point of the seams of the S_0/S_1 and S_1/S_2 CIs. These seams will be investigated below, cf. item x. The existence of this triple degeneracy is implied by the coexistence of three different reaction coordinates from the *syn*-A' form of C_5H_4NH via three different $TS_{biradical}$ $1A'$, $TS_{inversion}$ $1A'$, and $TS_{biradical}$ $1A''$ to the *anti*-A' form.[34] The energy of $S_0/S_1/S_2$ CI ($1A'/1A''/2A'$) relative to the potential minimum, $\Delta E = 3.46$ eV, is larger than $\Delta E = 2.80$ eV for S_0/S_1 CI ($1A'/1A''$), because, in general, $V_2 \geq V_1 \geq V_0$. For comparison, the vertical excitation energy for Franck−Condon transition from the *syn*-A' or *anti*-A' forms of C_5H_4NH (S_0) to the S_1 state is 4.47 eV, which is enough to reach all of these funnels and transition states.

Step 2: After location of two representatives of the CIs, we define convenient molecular-symmetry C_{2v}(M)-adapted coordinates $s = \{s_k\}$. The different geometries of the syn and anti forms of C_5H_4NH, the three TSs, and the CIs (Figure 3) show that one would need, in principle, many such coordinates s_k to describe motions between these configurations in detail. In view of our goal to demonstrate MS effects on NACTs and CIs as a proof of principle, the criteria for our choice of the s_k are less ambitious: We shall choose only two coordinates $s = \{s_1,s_2\}$ while freezing all the others; this is of course at the expense of covering the whole configuration space for all of the stationary points and all CIs of V_0. Instead, we focus on a scenario for large amplitude motions which start in the domain close to the syn form of C_5H_4NH, say after Franck−Condon (FC) excitation from S_0 to S_1, via the CI with smallest energy, i.e., S_0/S_1 CI ($1A'/1A''$), to the anti form in the electronic ground state S_0. Since S_0/S_1 CI ($1A'/1A''$) is close to $TS_{biradical}$ A'' for torsional motion from the syn form to the anti form of C_5H_4NH, cf. Figure 3, one of our molecular-symmetry-adapted coordinates should describe torsional motion.

Before giving a precise definition for the torsion angle and also for the second MS-symmetry-adapted coordinate, let us first consider how to "freeze" the complementary coordinates. For this purpose, we note that all of the structures shown in Figure 3 have similar C_5H_4N fragments; it will, therefore, be reasonable to freeze the coordinates of the C_5H_4N fragment in a C_{2v}(M) symmetry-adapted manner. There are various ways to do that. Our choice is based on the observation that, for the syn form of C_5H_4NH, the C_5H_4N fragment is planar (local C_s symmetry), but it does not have another perpendicular symmetry plane. In contrast, for S_0/S_1 CI ($1A'/1A''$), the five-membered carbon ring turns out to be not exactly but almost planar. More specifically, here the shape of the C_5H_4NH fragment looks like the symmetrical (C_s) wings of a butterfly folded away from the planar reference plane, by just 0.0367 radians (2.1°), with the CN bond as the "head of the butterfly", in the (local) vertical symmetry plane between the "wings". The two limiting albeit very similar geometries of the C_5H_4N fragment for the syn and anti forms as well as for S_0/S_1 CI ($1A'/1A'$) suggest, as a compromise, that this fragment should be frozen such that it has both perpendicular symmetry planes; i.e., it should have local C_{2v} symmetry, with the nuclear coordinates close to those of the limiting forms. For simplicity, we freeze all bond lengths and bond angles of the "butterfly" form of S_0/S_1 CI ($1A'/1A'$), except that the "wings" are rotated just slightly by those 0.0367 radians such that the C_5H_4 ring becomes planar; at the same time, the "head", i.e., the CN bond, is also rotated by just 0.004 radians into the plane of the C_5H_4 fragment. As a consequence, the local symmetry of the C_5H_4N fragment becomes C_{2v}, with the CN axis as the (local) C_2 axis. The distance of the proton of the NH bond from this CN axis is $r = 1.0$ Å. Figure 3 shows that all geometries of the C_5H_4N fragment are similar to this C_{2v} structure, not only for S_0/S_1 CI ($1A'/1A''$) but also for all of the other stationary points of V_0. Furthermore, Figure 1b shows that this C_{2v} geometry is robust with respect to all symmetry operations E, (12), E^*, and (12)* of C_{2v}(M); i.e., this geometry of the C_5H_4N fragment is described implicitly in terms of frozen, symmetry-adapted coordinates, which need not be specified, however, because they are irrelevant for the purpose of this paper. With this implicit definition of the frozen coordinates, the symmetry-adapted torsional angle φ and the complementary "radial" coordinates are defined as two cylindrical coordinates for rotation of the proton of the NH bond around the CN axis, relative to the C_5H_4N (C_{2v}) fragment. Their (global) IREPs are A_2 and A_1, respectively, cf. Table 1. The "prize" for this reasonable and rather simple choice of just two C_{2v}(M)-adapted coordinates is that motions along $s = \{r, \varphi\}$ may approach geometries of the syn and anti forms of C_5H_4NH as well as S_0/S_1 CI ($1A'/1A''$) rather closely but not perfectly. For example, the syn and anti forms and the S_0/S_1 CI ($1A'/1A''$) are approximated for $\{r, \varphi\} = \{1.0$ Å, 0$\}$, $\{1.0$ Å, $\pm\pi\}$, and $\{1.0$ Å, $\pi/2\}$, respectively, but the energies 0.47 and 2.69 eV differ from the exact references, 0.00 and 2.80 eV, respectively.

Step 3: Using the C_{2v}(M)-adapted coordinates $\{r, \varphi\}$, the results for the quantum chemistry calculations of the adiabatic

PES V_j, $j = 0, 1, 2$, versus φ are shown in Figure 5a, b, and c for three different values of $r = 1.0$, 0.8, and 1.2 Å, respectively. The value $r = 1.0$ Å corresponds to the case of S_0/S_1 CI ($1A'/1A''$); see step 1. Accordingly, Figure 5a shows a near degeneracy of V_0 and V_1 at $\{r = 1.0$ Å, $\varphi = \pi/2\}$ with mean energy $(V_0 + V_1)/2 = 2.69$ eV and energy gap $V_1 - V_0 \leq 0.03$ eV, which confirms the signature of S_0/S_1 CI ($1A'/1A''$) which has been located in step 1. From now on, we shall refer to this as the "first" (subscript 1) $CI_1^{0,1}$, using the notation for the "global" MS C_{2v}(M); see section II. The corresponding coordinates are $[\{r^{0,1} \approx 1.0$ Å, $\varphi^{0,1} = \pi/2\}]_1$. Application of the symmetry operations E, (12), E^*, and (12)* generates the complete set of MS-adapted $CI_1^{0,1}$ and $CI_2^{0,1}$, where $CI_2^{0,1}$ is located at $[\{r^{0,1} \approx 1.0$ Å, $\varphi^{0,1} = -\pi/2\}]_2$.

Incidentally, Figure 5a also shows a near degeneracy of V_1 and V_2, with mean energy $(V_1 + V_2) = 3.96$ eV and gap $V_2 - V_1 \leq 0.02$ eV, located at $\{r = 1.0$ Å, $\varphi = 0.628(36°)\}$. By extrapolation, we conclude that this is a signature of a conical intersection $CI_1^{1,2}$ located at $[\{r^{1,2} \approx 1.0$ Å, $\varphi^{0,1} \approx 0.628\}]_1$. The symmetry operations (12), E^*, and (12)* generate the complete set of symmetry-adapted CIs including $CI_2^{1,2}$ at $[\{r^{1,2} \approx 1.0$ Å, $\varphi^{1,2} \approx -\pi + 0.628 = -2.513(-144°)\}]_1$, $CI_3^{1,2}$ at $[\{r^{1,2} \approx 1.0$ Å, $\varphi_2^{0,1} \approx -0.628(-36°)\}]_1$, and $CI_4^{1,2}$ at $[\{r^{1,2} \approx 1.0$ Å, $\varphi^{1,2} \approx \pi - 0.628 = 2.513(144°)\}]_4$; compare Figures 1b and 5a.

Figure 5b for the adiabatic PES at $r = 0.8$ Å shows two molecular-symmetry-adapted avoided crossings of V_0 and V_1 which remind us of the $CI_1^{0,1}$ and $CI_2^{0,1}$ at $\varphi = \pi/2$ and $-\pi/2$, respectively. The energy gap $V_1(r = 0.8$ Å, $\varphi = \pi/2) - V_0(r = 0.8$ Å, $\varphi = \pi/2)$ at the avoided crossing is, however, much larger than $V_1(r = 1.0$ Å, $\varphi = \pi/2) - V_0(r = 1.0$ Å, $\varphi = \pi/2) = 0.03$ eV for the near degeneracy close to $CI_1^{0,1}$. In addition, Figure 5b also shows four C_{2v}(M)-adapted near degeneracies of V_1 and V_2 which remind us of $CI_g^{1,2}$, $g = 1, 2, 3, 4$, which have been discovered in Figure 5a. Specifically, in Figure 5b, $CI_1^{1,2}$ is located at $[\{r^{1,2} \approx 0.8$ Å, $\varphi^{0,1} \approx 1.047(60°)\}]_1$. The symmetry operations of C_{2v}(M) applied to $CI_1^{1,2}$ generate the other three $CI_g^{1,2}$, $g = 2, 3, 4$, analogous to Figure 5a. It is important to note that the values of the radial and torsional coordinates $[\{r^{1,2}, \varphi^{1,2}\}]_g$ of the symmetry-adapted CI_g are different in Figure 5a and b. In contrast, both figures point to the same values of the torsional angles $\varphi = \pi/2$ or $-\pi/2$ for $CI_1^{0,1}$ and $CI_2^{0,1}$, respectively.

Figure 5c for the adiabatic PES at $r = 1.2$ Å shows avoided crossings not only for V_0 and V_1 but also for V_1 and V_2. Again, these point to neighboring sets of symmetry-adapted $CI_g^{0,1}$, $g = 1, 2$, and $CI_g^{1,2}$, $g = 1, 2, 3, 4$, similar to those which have been discovered and confirmed in Figure 5a and b, respectively. Apparently, the locations of the neighboring $CI_g^{0,1}$ are at the same torsional angles $\varphi = \pi/2$ and $-\pi/2$, whereas pairs of corresponding torsional angles for $CI_g^{1,2}$ have moved to and merged at $\varphi = \pi/2$ and $\varphi = -\pi/2$.

The results shown in Figure 5a already imply an empirical working hypothesis; i.e., the seams of the conical intersections $CI_g^{0,1}$ in the (r, φ)-plane are restricted to $\varphi = \pi/2$ or $\varphi = -\pi/2$, whereas the seam of the $CI_g^{1,2}$ extends over all values of φ. A systematic analysis will be added in item x.

(iv) Using the symmetry-adapted coordinates $\{r, \varphi\}$, the NACTs are defined, in accord with eq 10, as

$$\tau_r^{i,j}(r, \varphi) = \langle \psi_i(r, \varphi) | \frac{\partial}{\partial r} \psi_j(r, \varphi) \rangle \tag{40}$$

and

$$\tau_\varphi^{i,j}(r, \varphi) = \langle \psi_i(r, \varphi) | \frac{\partial}{\partial \varphi} \psi_j(r, \varphi) \rangle \tag{41}$$

In practice, they are calculated by means of finite differences; specifically, we employ the approximations

$$\tau_r^{i,j}(r, \varphi) \approx \frac{1}{2\Delta r}[\langle \psi_i(r, \varphi) | \psi_j(r + \Delta r, \varphi) \rangle - \langle (\psi_i(r, \varphi) | \psi_j(r - \Delta r, \varphi) \rangle] \tag{42}$$

and

$$\tau_\varphi^{i,j}(r, \varphi) \approx \frac{1}{2\Delta \varphi}[\langle \psi_i(r, \varphi) | \psi_j(r, \varphi + \Delta\varphi) \rangle - \langle \psi_i(r, \varphi) | \psi_j(r, \varphi - \Delta\varphi \rangle] \tag{43}$$

which are valid to third orders of the parameters Δr and $\Delta\varphi$ for the finite differences. The choice of these parameters is made considering two opposite requirements: on one hand, the request of numerical convergence suggests very small values of Δr and $\Delta\varphi$; in any case, they should be much smaller than the widths of any sharp peaks which may appear in the NACTs, in particular close to the CIs. On the other hand, they should not be chosen smaller than the limits which are imposed by the sensitivity of the quantum chemistry calculations of the electronic wave functions with respect to very small shifts of the nuclear positions. As a compromise, we employ the values $\Delta r = 0.0189$ Å and $\Delta\varphi = 1.74 \times 10^{-4}$ (0.01°) for the subsequent results.

Let us first focus on the quantum chemical results for the torsional NACTs; some complementary results for the radial NACTs $\tau_r^{i,j}$ will be discussed in item xii. The $\tau_\varphi^{i,j}(r, \varphi)$, $r = 1.0$, 0.8, and 1.2 Å, in the domain $0 \leq \varphi \leq \pi/2$ are shown in Figure 6a, b, and c, respectively. For the discusssion, we also refer to the correponding near degeneracies versus avoided crossings of the V_j which point to rather close versus not so close neighboring locations of the CIs, as discovered in Figure 5a, b, and c, respectively. For example, for $r = 1.0$ Å, Figure 5a allowed us to locate $CI_1^{0,1}$ and $CI_1^{1,2}$; see item ii. Figure 6a shows corresponding large peaks of the NACTs $\tau_\varphi^{0,1}$ and $\tau_\varphi^{1,2}$ close to the $CI_1^{0,1}$ and $CI_1^{1,2}$, respectively, with rapid decay as one moves away from the CIs. This is in accord with the pole property of the NACTs close to CIs, eq 24. The sign of these peaks of the NACTs close to these "first" $CI_1^{0,1}$ and $CI_1^{1,2}$ are arbitrary, because the signs of the underlying electronic wave functions $\psi_j(s_e; \{r, \varphi\})$, $j = 0, 1, 2$, are arbitrary. As a convention, we have assigned positive signs to the NACTs close to the "first" CIs, cf. Figure 6a. In contrast, there is no near degeneracy between V_0 and V_2 in the restricted domain $\{r = 1.0$ Å, $0 \leq \varphi \leq \pi/2\}$; the maximum absolute value of the corresponding $\tau_\varphi^{0,2}$ is, therefore, much smaller than the peak values of $\tau_\varphi^{0,1}$ or $\tau_\varphi^{1,2}$. The signs of $\tau_\varphi^{0,2}$ are no longer arbitrary, however; i.e., they depend on the given assignments for $\tau_\varphi^{0,1}$ and $\tau_\varphi^{1,2}$ because all of the torsional $\tau_\varphi^{i,j}$ involve the same electronic wave functions labeled $i = 0, 1$ and $j = 1, 2$ $(i < j)$. As a consequence, $\tau_\varphi^{0,2}$ is negative in the domain close to $CI_1^{1,2}$ such that the values of $\tau_\varphi^{0,2}$ and $\tau_\varphi^{0,1}$ interchange close to $CI_1^{1,2}$, cf. Figure 6a. As discussed in section II, item vii c, this points to a switch of the characters of the electronic wave functions $\psi_1(s_e; \{r = 1.0$ Å, $\varphi\})$ and $\psi_2(s_e; \{r = 1.0$ Å, $\varphi\})$ close to $CI_1^{1,2}$.

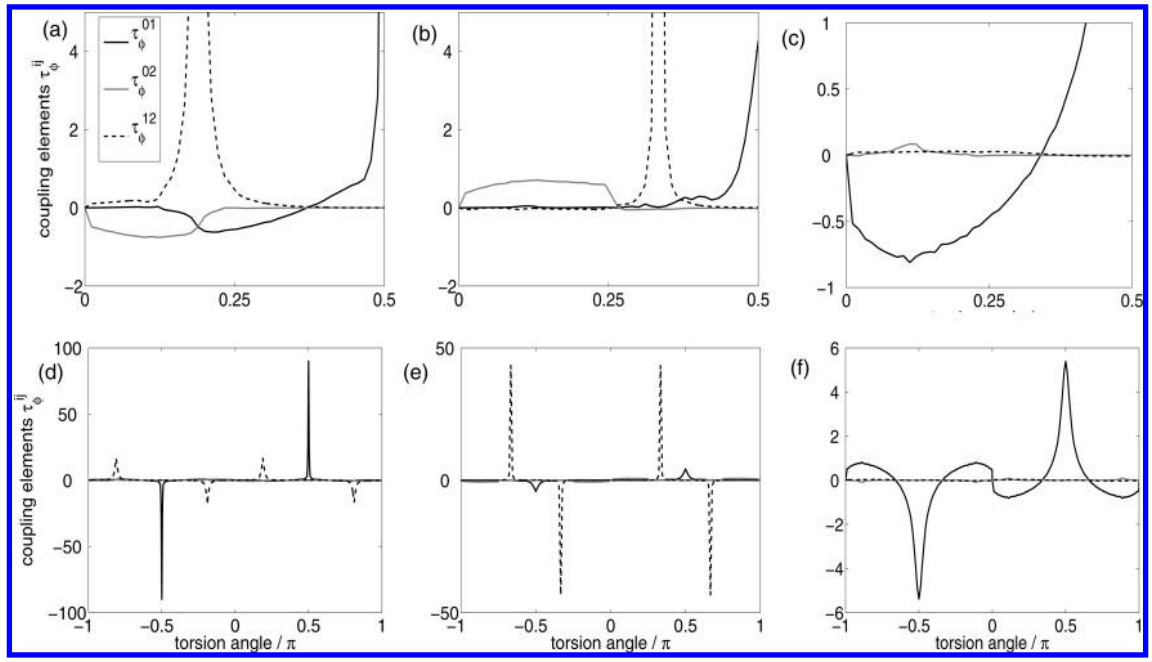

Figure 6. Torsional nonadiabatic coupling terms (NACTs) of C_5H_4NH, $\tau_\varphi^{0,1}(r,\varphi)$ (black continuous lines), $\tau_\varphi^{1,2}(r,\varphi)$ (dashed lines), and $\tau_\varphi^{0,2}(r,\varphi)$ (gray continuous lines) in the domains $0 \le \varphi \le \pi/2$ (panels a−c) and $-\pi \le \varphi \le +\pi$ (panels d−f) for $r = 1.0$ Å (panels a and d), $r = 0.8$ Å (panels b and e), and $r = 1.2$ Å (panels c and f), in units of 1/radians. Note the different scales, i.e., on one hand, the "blown-up" panels a−c discover details such as the crossing of $\tau_\varphi^{0,1}$ and $\tau_\varphi^{0,2}$ which cannot be resolved in panels d−f. On the other hand, the "global" panels d−f demonstrate the patterns of the signs of the peaks of the NACTs, in accord with their irreducible representations in the frame of the "global" molecular symmetry group C_{2v}(M), i.e., B_1 for $\tau_\varphi^{0,1}$ and $\tau_\varphi^{0,2}$ as well as B_2 for $\tau_\varphi^{1,2}$, c.f. Table 1.

For the other examples, $r = 0.8$ and 1.2 Å, the signs of the peaks (or the relative maxima) of the NACTs $\tau_\varphi^{0,1}$ and $\tau_\varphi^{1,2}$ are also set to be positive, as for $r = 1.0$ Å; compare parts b and c of Figure 6 with part a, respectively. The consistency of this assignment will be discussed in item xii. Thus, for $r = 0.8$ Å, Figure 6b shows a large positive peak of $\tau_\varphi^{1,2}$ close to $CI_I^{1,2}$ which has been deduced from the near degeneracy of V_1 and V_2 close to $\varphi = 1.047$ (60°), cf. Figure 5b. In contrast, the increase of the energy gap between V_1 and V_0 which has been interpreted as avoided crossing, suggesting that this is further away from $CI_I^{0,1}(r = 0.8, \varphi)$, causes strong depletion of the corresponding peak value of $\tau_\varphi^{0,1}$; compare parts b and a of Figure 6. We extrapolate a general trend from near degeneracies to avoided crossings with increasing energy gaps between 1-d cuts of the PES; these signatures of the CIs are located at increasing distances from the corresponding CIs, causing systematic decreases of the peak values of the correponding NACTs, in accord with the pole property, eq 24. This conjecture is confirmed by the results shown in Figures 5c and 6c for $r =$ 1.2 Å: the previous near degeneracies (Figure 5a for $r = 1.0$ Å) are transformed into avoided crossings, not only for V_0 and V_1 (as in Figure 5b) but even more drastically for V_1 and V_2. Figure 6c shows that, indeed, the peak value of $\tau_\varphi^{0,1}$ at $\{r = 1.2$ Å, $\varphi = \pi/2\}$ is much smaller than at $\{r = 1.0$ Å, $\varphi = \pi/2\}$, Figure 6a. Moreover, the peak for $\tau_\varphi^{1,2}$ which was so obvious in Figure 5a and b has decayed to a marginal maximum value which is hardly noticeable in Figure 6c.

Before moving on to the next items (v, etc.), we note that close to the boundaries of Figure 6a−c, i.e., at $\varphi = 0$ and $\pi/2$, some of the $\tau_\varphi^{i,j}$ have decayed to very small values, below the accuracy of the quantum chemistry based method for calculating the NACTs. In these cases, quantum chemistry *per se* is not sufficient to determine the signs of the NACTs in these neighborhoods and, therefore, also not in other connected domains. The solution of this dilemma is postponed until item xi, i.e., after conquering the molecular symmetry properties of the NACTs and CIs.

(v−vii) It is now straightforward to solve the combined task of the assignment of the IREPs of the NACTs of C_5H_4NH, together with their nodal patterns, based on the general theorems and properties which have been derived and summarized in section II, in the frame of the molecular symmetry group C_{2v}(M). Let us first recall that two of these properties, i.e., the quantization rule and the pole property, eqs 22 and 24, apply for the model of two-state systems.[1] The exclusive peaks of the NACTs $\tau_\varphi^{0,1}(\{r = 1.0$ Å, $\varphi\})$ and $\tau_\varphi^{1,2}(\{r = 1.0$ Å, $\varphi\})$ in narrow domains close to the $CI_I^{0,1}$ and $CI_I^{1,2}$ demonstrate the approximate validity of the two-state scenario; i.e., there are apparently no other CIs which interfere with $CI_I^{0,1}$ or $CI_I^{1,2}$ close to $[\{r^{0,1}, \varphi^{0,1}\}]_1$ and $[\{r^{1,2}, \varphi^{1,2}\}]_1$, respectively, cf. Figure 6a. This example for $r = 1.0$ Å is sufficient for the derivation of the IREPs of the NACTs, because these are global properties of the MS group C_{2v}(M) of C_5H_4NH; i.e., once they are determined for the special case $r = 1.0$ Å, they apply automatically also to other values the MS-adapted coordinates.

Let us start from the discovery of the $CI_I^{0,1}$ based on the LH theorem (=S_0/S_1 CI ($1A'/1A''$), item ii) at $\varphi^{0,1} = \pi/2$. This location implies immediately that $\Gamma(\tau_\varphi^{0,1}) = B_1$, cf. section II (vii). We recall that the derivation of this result exploits the quantization rule (22) and the pole property (24), in the frame of the two-state model which is approximately valid as discussed above. Moreover, the general theorem (15) immediately relates the IREP B_1 of $\tau_\varphi^{0,1}$ to the IREPs of all of the other NACTs $\tau_k^{0,1}$, for the same states $i, i + 1 = 0, 1$. Specifically, the radial NACT has $\Gamma(\tau_r^{0,1}) = B_2$, whereas the Cartesian ones (eq 5) have $\Gamma(\tau_x^{0,1}) = A_1$ and $\Gamma(\tau_y^{0,1}) = A_2$. Table 1 also lists the corresponding sign patterns for the peaks of the NACTs, as well as their nodal patterns. As an example, $\tau_\varphi^{0,1}(\{r,\varphi\})$ should have opposite signs of the peaks for $\varphi = \pi/2$ and $-\pi/2$, and corresponding nodes at $\varphi = 0$ and $\pm\pi$.

Next, we recall that the NACTs $\tau_{\varphi}^{0,1}(r = 1.0, \varphi)$ and $\tau_{\varphi}^{0,2}(r = 1.0$ Å, $\varphi)$ interchange close to $CI_1^{1,2}$ which is located at $[\{r^{1,2} \approx 1.0$ Å, $\varphi^{1,2} \approx 0.628(36°)\}]_1$, cf. Figure 6a. The general properties of the NACTs then imply that the IREPs of $\tau_{\varphi}^{0,1}$ and $\tau_{\varphi}^{0,2}$ are the same, i.e., $\Gamma(\tau_{\varphi}^{0,2}) = \Gamma(\tau_{\varphi}^{0,1}) = B_1$, cf. eqs 25−27. Likewise, for each pair of the NACTs $\tau_k^{0,2}$ and $\tau_k^{0,1}$ with respect to the other MS-adapted coordinates $s_k = r, \varphi$ or x, y, the IREPs are also the same, c.f. theorem 15. As a consequence, the pairs of NACTs $\tau_k^{0,2}$ and $\tau_k^{0,1}$ have the same nodal patterns; for example, $\tau_{\varphi}^{0,2}$ should have nodes at $\varphi = 0$ and at $\varphi = \pm\pi$, same as for $\tau_{\varphi}^{0,1}$, *vide infra*.

Finally, we use the general theorem 17 which includes the special case (19) to determine the IREP of the NACT which is still "missing", $\tau_{\varphi}^{1,2}$. The result is $\Gamma(\tau_{\varphi}^{1,2}) = A_2$; see the discussion of eq 19 in section II. Using this as a reference, the IREPs of $\tau_k^{1,2}$ for the other MS-adapted coordinates s_k are determined, again using theorem 15. The results for the IREPs, the sign patterns of the peaks, and the nodal patterns for all of the NACTs τ_k^{ij}, with respect to all coordinates $k = r, \varphi, x, y$ and for the three lowest electronic singlet states $i = 0, 1, j = 1, 2, i < j$ are listed in Table 1. For example, $\tau_{\varphi}^{1,2}$ should have nodes not only at $\varphi = 0$ and $\varphi = \pm\pi$ but also at $\varphi = \pm\pi/2$. It is impossible to deduce all of these nodal patterns, which are a property of the MS symmetry of C_5H_4NH, from the quantum chemistry results shown in Figure 6a−c. For example, the values of NACTs $\tau_{\varphi}^{0,1}(\{r = 1.0$ Å, $\varphi\})$ close to $\varphi = \pi/2$, i.e., far away from $CI_1^{1,2}$, are compatible with a node or with no node at $\pi/2$, because they are below the accuracy of the method for calculating the NACTs.

(viii) The charges $e_1^{0,1}$ and $e_1^{1,2}$ of the "first" $CI_1^{0,1}$ and $CI_1^{1,2}$, are calculated by means of planar contour integrals of the tangential NACTs along loops around the CIs, cf. eq 22. We assume that one can construct loops around the single CI_1's for these contour integrals such that they consist of segments for the torsional NACTs with large positive values close to the CI_1's, as well as other segments for small values of NACTs far away from the CI; see, e.g., loop L_1 illustrated in Figure 2. Our assignment of the positive sign for the angular NACTs $\tau_{\varphi}^{0,1}$ and $\tau_{\varphi}^{1,2}$ with large absolute values close to the "first" $CI_1^{0,1}$ and $CI_1^{1,2}$ implies, therefore, by definition, that the charges $e_1^{0,1}$ and $e_1^{1,2}$ of the "first" CI_1's are always equal to 1. This is also confirmed by numerical calculation of the contour integrals for convenient loops. For example, for $CI_1^{0,1}$, we construct a loop which consists of two half-circles ($0 \le \varphi \le \pi$) with radii $r = 1.2$ Å and $r = 1.0$ Å plus two connecting lines on the x-axis, from $x = -1.2$ Å until -1.0 Å and from $x = 1.0$ until 1.2 Å; the value of the corresponding contour integral agrees with $+\pi$ within numerical accuracy; i.e., the charge of $CI_1^{0,1}$ is $e_1^{0,1} = 1$.

(ix) The assignment of the IREPs of the sets of MS-adapted $CI_g^{0,1}$ ($g = 1, 2$) and $CI_g^{1,2}$ ($g = 1, 2, 3, 4$) depends on their charges $e_g^{0,1}$ and $e_g^{1,2}$, respectively. The latter are determined by the signs of contour integrals of the tangential NACTs along suitable loops which surround these CIs. The procedure has been illustrated for two examples, cf. section II, item ix. For the present system C_5H_4NH, $CI_1^{0,1}$ has been located at $[\{r^{0,1} \approx 1.0$ Å, $\varphi = \pi/2\}]_1$, using the LH theorem (cf. items ii and iii); this is the scenario of the first example. Hence, we can adapt the results of section II, item ix. Accordingly, $CI_1^{0,1}$ and $CI_2^{0,1}$ have opposite charges $e_2^{0,1} = -e_1^{0,1} = -1$, with corresponding IREP B_1, the same as for $\tau_{\varphi}^{0,1}$.

Now let us apply the analogous procedure to determine the IREP of $CI_g^{1,2}$; accordingly, we construct a loop (similar to L_4 in Figure 2c) around $CI_1^{1,2}$ as well as the MS-adapted loops around the other $CI_g^{1,2}$, $g = 2, 3, 4$. The IREPs A_2 of $CI_{\varphi}^{1,2}$ and A_1 of $\tau_r^{1,2}$, with corresponding patterns of the signs, as illustrated in Table 1, then yield alternating signs of the contour integrals, hence alternating charges $e_1^{1,2} = -e_2^{1,2} = e_3^{1,2} = -e_4^{1,2}$, identical to the sign patterns of $\tau_{\varphi}^{1,2}$, cf. Table 1. As a consequence, the IREP of $CI^{1,2}$ is A_2, again the same as for $\tau_{\varphi}^{1,2}$.

(x) In section II, item x, we have shown that, if the first $CI_1^{i,i+1}$ between adiabatic PES V_i and V_{i+1} is located at $[\{r^{i,i+1}, \varphi^{i,i+1} = \pi/2\}]_1$, then the entire seam of $CI^{i,i+1}$ in the (r, φ)-plane is restricted to $\varphi = \pi/2$ or $-\pi/2$, for $CI_1^{i,i+1}$ and $CI_2^{i,i+1}$, respectively. The location of $CI_1^{0,1}$ between the electronic ground and first excited states at $[\{r^{0,1} \approx 1.0$ Å, $\varphi^{0,1} = \pi/2\}]_1$ by means of the LH theorem fulfills this condition; hence, we conclude that the signatures of the 3N-8 dimensional seam of $CI^{0,1}$ in the (r, φ)-plane is restricted to two points corresponding to perpendicular geometries of C_5H_4NH, $\varphi = \pi/2$ or $-\pi/2$. In contrast, the seam of $CI^{1,2}$ with $CI_1^{1,2} \neq \pm\pi/2$ in the (r, φ)-plane is not restricted to $+\pi/2$ and $-\pi/2$, see Figures 5a, 5b.

Our quantum chemistry results confirm these different topologies of the seams of $CI^{0,1}$ and $CI^{1,2}$. First, we carried out a systematic search for any exceptions in the (r, φ)-plane, but we could not discover any degeneracies or near degeneracies of V_0 and V_1 for any geometries of C_5H_4NH other than the perpendicular one, $\varphi_0 = +\pi/2$ or $-\pi/2$. Second, the results shown in Figure 6a and b already suggest that the seam of $CI_1^{1,2}$ exists for two values of $\varphi^{1,2} \approx 0.628(36°)$ and $1.047(60°)$, for $r^{1,2} \approx 1.0$ and 0.8 Å, respectively. By extrapolation, one can also determine (near) degeneracies of V_1 and V_2 for arbitrary fixed values $\varphi^{1,2}$, by systematic variations of r; i.e., the seam of $CI^{1,2}$ appears as a line in the (r, φ)-plane. The seam of $CI^{1,2}$ in the domain $0 < \varphi \le \pi/2$ can be extended to the full cycle, $-\pi \le \varphi \le \pi$, using the MS operations (12), E^*, and (12)*, cf. Figure 1. Further investigations of the seams of the CIs will be published elsewhere; see also the discussion in refs 43, 44.

(xi) We are now ready to construct the NACTs $\tau_{\varphi}^{ij}(r, \varphi)$ (and similarly the $\tau_k^{ij}(r,\varphi)$ for the other MS-adapted coordinates s_k ($= r, x, y$)) in the global domain $-\pi \le \varphi \le \pi$, by combining the results for the IREPs of the NACTs with the quantum chemistry results for the restricted, albeit representative domain $0 \le \varphi \le \pi/2$ which have been documented in Figure 6a−c. This task requires two steps. First, we apply the symmetry operations (12), E^*, and (12)* (Figure 1) to generate the same absolute values of the NACTs at the MS-adapted coordinates (13). Second, the signs of the NACTs are determined according to their IREPs, as shown in Table 1. Note that this procedure applies for all radii r, because the IREPs of the NACTs are a global property of the MS $C_{2v}(M)$ of C_5H_4NH; i.e., they are not restricted to any special value of r (irrespective of the fact that a special value, $r = 1.0$ Å, was used to locate the first $CI_1^{0,1}$, using the LH theorem, cf. item ii). The results, i.e., $\tau_{\varphi}^{ij}(r, \varphi)$ for $i = 0, 1, j = 1, 2, i < j$ in the domain $-\pi \le \varphi \le \pi$ are shown in Figures 6d, e, and f for $r = 1.0$, 0.8, and 1.2 Å, respectively. The first step, i.e., determination of the absolute values, is based on quantum chemistry per se. In contrast, quantum chemistry cannot determine the signs of the NACTs beyond the boundaries of the representative domain, $0 \le \varphi \le \pi/2$, if the absolute values of the NACTs at the boundaries are below the intrinsic accuracy of the method. This dilemma is solved by combining the quantum chemistry results with the results for the IREPs of the NACTs.

(xii) Finally, we present several tests of self-consistency for the results which have been achieved in items i−xi.

First, we recall that the value of the contour integral for the loop which consists of two half circles with radii $r = 1.2$ and 1.0 Å, plus two connecting segments on the x-axis, around $CI_1^{0,1}$

(as explained above) is equal to π, allowing the assignment of its charge $e_{\Gamma}^{0,1} = 1$, within numerical accuracy; this is in accord with eq 22. Likewise, the value of the analogous contour integral for the loop with corresponding radial parameters $r = 1.0$ and 0.8 Å, which does not include $CI_{\Gamma}^{0,1}$, is equal to zero, in accord with eq 23. These results confirm the self-consistency of the assignments of the same, positive signs of the values of the peaks of the $\tau^{0,1}(\{\varphi = \pi/2, r\})$ for the three cases, $r = 1.0$, 0.8, and 1.2 Å, cf. Figure 6a−c.

Second, theorem 15 relates the IREPs of the torsional NACTs $\tau_{\varphi}^{i,j}$ to the IREPs of all other $\tau_{k}^{i,j}$; see also Table 1. Accordingly, the IREPs of the radial NACTs $\tau_r^{0,1}$, $\tau_r^{0,2}$, and $\tau_r^{1,2}$ should be B_2, B_2, and A_1, implying nodes for $\tau_r^{0,1}(\{r, \varphi\})$ and $\tau_r^{0,2}(\{r, \varphi\})$ at $\varphi = \pi/2$ but no node for $\tau_r^{1,2}(\{r, \varphi\})$. Quantum chemical calculations of the radial NACTs confirm this symmetry property of the radial NACTs, as demonstrated in Figure 7.

The third test of the self-consistency of the IREPs of the torsional NACTs $\tau_{\varphi}^{i,j}$ is provided by the quantization rule for the so-called $N \times N$ topological matrix $\mathbf{D}(r)$ which depends on the NACTs. Specifically, $\mathbf{D}(r)$ is defined in terms of the $N \times N$ adiabatic-to-diabatic transformation (ADT) matrix, also called the $\mathbf{A}$ matrix (see ref 1, Chapter 4, and refs 37 and 38)

$$\mathbf{A}(r; \varphi) = \mathscr{P}\exp[-\int_{\varphi_0}^{\varphi} d\varphi \boldsymbol{\tau}_{\varphi}(r; \varphi)]\mathbf{A}(r; \varphi_0) \quad (44)$$

where $\boldsymbol{\tau}_{\varphi}$ is the antisymmetric $N \times N$ nonadiabatic coupling matrix with elements $\tau_{\varphi}^{i,j}$, $i, j = 0, \ldots, N - 1$, and $\mathscr{P}$ is the ordering operator. In the applications below, we consider the states S_0, S_1, and S_2, thus, $N = 3$; the starting point is $\varphi_0 = -\pi$, and the $\mathbf{A}$ matrix at the starting point is defined as the unity matrix, for convenience. Integration along a circular closed loop $L(r)$ with radius r, i.e., from φ_0 to $\varphi_0 + 2\pi$, yields the topological matrix $\mathbf{D}(r)$[13,28]

$$\mathbf{D}(r) = \mathbf{A}(r, 2\pi) = \mathscr{P}\exp[-\int_{\varphi_0}^{\varphi_0+2\pi} d\varphi \boldsymbol{\tau}_{\varphi}(r; \varphi)]\mathbf{A}(r; \varphi_0) \quad (45)$$

It can be shown that $\mathbf{D}(r)$ is diagonal if the N states form a quasi-Hilbert subspace in the region surrounded by $L(r)$. Furthermore, $\mathbf{D}$ is by construction an orthogonal matrix. Since it is diagonal and orthogonal, its diagonal elements are equal either to $+1$ or to -1. Moreover, it can be shown that the number of (-1)'s has to be even (ref 1, lemma 5.3 on p 119). We note in passing that the $\mathbf{A}$ matrix is called the ADT matrix because it may be used to transform the diagonal matrix $\mathbf{V}(r, \varphi)$ for the adiabatic PES, $V(r, \varphi)_{i,j} = V_j(r, \varphi)\delta_{i,j}$, into the diabatic potential matrix

$$\mathbf{W}(r, \varphi) = \mathbf{A}(r, \varphi)^{\dagger}\mathbf{V}(r, \varphi)\mathbf{A}(r, \varphi) \quad (46)$$

Since $\mathbf{A}(r, \varphi)$ is defined for torsional contours, $\mathbf{W}(r, \varphi)$ is also defined for these contours. The quantization rule for the topological matrix guarantees that, in the limit of the closed circular contour, the diabatic matrix elements are single-valued, $\mathbf{W}(r, \varphi) = \mathbf{W}(r, \varphi + 2\pi)$. Applications of the diabatic potentials based on the NACTs with proper IREPs for the MS C_{2v}(v) to quantum dynamics simulations of photoexcited C_5H_4NH will be presented elsewhere.

This quantization rule of the $\mathbf{D}$ matrix is a very sensitive test for the quantum chemical calculations of the NACTs in the representative domain $0 \le \varphi \le \pi/2$ (Figure 6a−c), as well as for the extensions to the global domain $-\pi \le \varphi \le \pi$ based on their IREPs (Figure 6d−f): Any quantum chemical calculation of the NACTs and assignment of their IREPs that does not lead to a diagonal $\mathbf{D}$ matrix with an even number of (-1)'s can be ruled out.

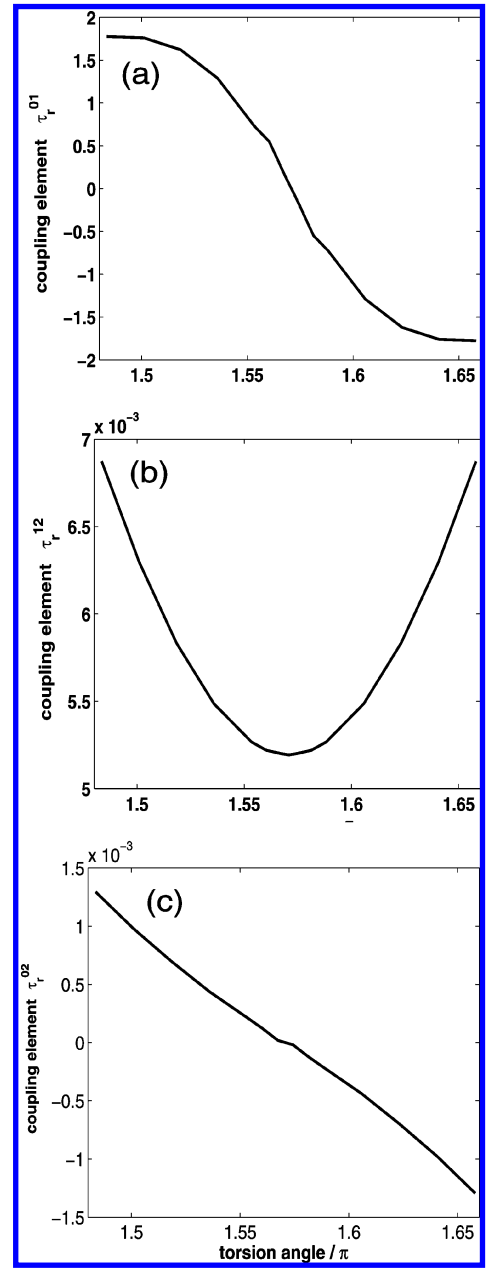

Figure 7. Quantum chemistry results for the nodal properties of the radial nonadiabatic coupling elements (NACTs) of C_5H_4NH, $\tau_r^{0,1}$ (a), $\tau_r^{1,2}$ (b), and $\tau_r^{0,2}$ (c), in a narrow domain close to $\pi/2$. Note the different scales. These results are consistent with their irreducible representations B_2, A_1, and B_2, respectively, as deduced by the theorem 15 for the NACTs in the frame of the molecular symmetry group C_{2v}(M), cf. Table 1.

Applications of the third self-consistency test for the NACTs and their IREPs are demonstrated in Figure 8. Specifically, Figure 8a−c, d−f, and g−i show the elements of the $\mathbf{A}(r, \varphi)$ matrix for $r = 1.0$, 0.8, and 1.2 Å, based on the NACTs $\tau_{\varphi}^{i,j}$ shown in Figure 6d, e, and f, respectively, in the domain $-\pi \le \varphi \le +\pi$. In the limit $\varphi \rightarrow \pi$, the ADT matrix approaches the topological matrix $\mathbf{D}(r)$. It is gratifying that the numerical values of $\mathbf{D}(r)$ satisfy the quantization rule perfectly.

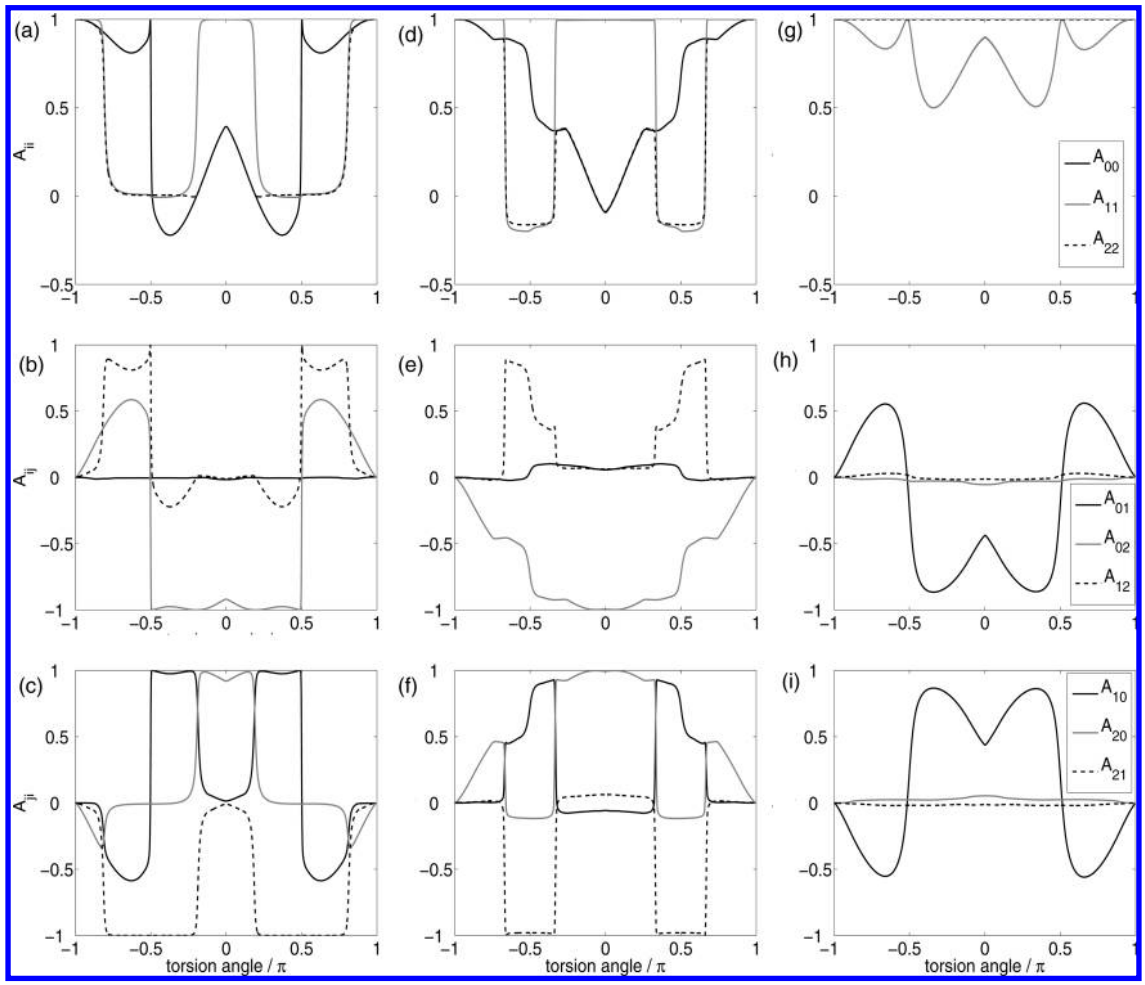

Figure 8. Elements of the A-matrices of C_5H_4NH as a function of φ for $r = 1.0$ Å (panels a−c), $r = 0.8$ Å (panels d−f), and $r = 1.2$ Å (panels g−i). Panels a, d, and g show the diagonal elements A_{00} (solid black lines), A_{11} (gray lines), and A_{22} (dashed lines). Panels b, e, and h and c, f, and i show the off-diagonal elements A_{01} (solid black lines), A_{02} (gray lines), and A_{12} (dashed lines) and A_{10} (solid black lines), A_{20} (gray lines), and A_{21} (dashed lines), respectively.

IV. Conclusions

This paper combines two fields of research: Quantum chemistry beyond Born−Oppenheimer,[1] and the theory of the molecular symmetry groups,[8] to the benefit of our understanding of the conical intersections CIs and the nonadiabatic coupling terms NACTs which mediate transitions between different nonadiabatic potential energy surfaces PES in molecules. Quantum chemistry has been developed as a method to determine the electronic structures of a molecule, depending on the positions of the nuclei in "local" environments, e.g., at or near stationary points of the potential energy surfaces PES such as potential minima or transition states. As a consequence, the results of quantum chemistry calculations, in particular the electronic states, have been classified traditionally according to the irreducible representations IREPs of the molecular point groups for the given local environment. The present work provides an extension of these symmetry assignments, from the IREPs for "local" molecular point groups to the "global" molecular symmetry MS group. This opens the door to investigations of molecular properties "beyond Born−Oppenheimer" in global molecular domains, e.g., mediated by large amplitude motions, such as isomerizations or torsions.

As a result of our investigation, we could discover several important properties of the CIs and the related NACTs with respect to molecular-symmetry-adapted coordinates. For example, if quantum chemistry calculations of the adiabatic potential energy surfaces $V_i(s)$ and $V_{i+1}(s)$ have localized the first $CI_1^{i,i+1}$ between these PES at $s = s_1^{i,i+1}$, then one can apply the symmetry operations $\hat{S}_g$, $g = 1, 2, \ldots, G$ of the MS in order to generate a complete set of MS-adapted $CI_g^{i,i+1}$ at different locations $s_g^{i,i+1} = \hat{S}_g s_1^{i,i+1}$.

The main effort of this paper has been for the determination of the irreducible representations IREPs of the NACTs and the CIs. For this purpose, we have derived the general theorems 15 and 17. Together with known properties of the NACTs related to the CIs,[1] in particular the quantization rule (22), the pole property (24), and in addition also the switching property (25), these theorems allow one to determine the IREPs of the NACTs and CIs, in the frame of the MS group. These IREPs imply several "global" properties, such as the patterns of the signs of the peak values of the NACTs close to the set of MS-adapted CIs, the nodal patterns of the NACTs, the signs or charges of the MS-adapted sets of CIs, and different topologies of the seams of the CIs in specific planes of MS-adapted coordinates depending on their IREPs. These "global" properties can in general not be derived by means of pure quantum chemistry; they are a result of its combination with the "global" MS group. For example, quantum chemistry can provide the same absolute values of the NACTs close to several symmetry-adapted potential minima supporting different isomers; the signs of these NACTs depend on their IREPs which are derived in this paper, in the frame of the MS group. Also, the "global"

MS property of the IREPs, together with theorem 15, implies that, in practice, it suffices to determine the IREPs of the NACT $\tau_k^{i,j}(s)$ with respect to a single symmetry-adapted coordinate s_k; this implies the IREPs of all other $\tau_{l'}^{i,j}(s)$, for all coordinates s.

The general theory and the resulting recipes for constructions of the NACTs and CIs with the proper IREPs in global domains, e.g., for torsional motions from the molecular syn to the anti isomer, have been demonstrated in detail for the simple model C_5H_4NH which has MS symmetry C_{2v}(M). The step-by-step approach should serve as an example for extended applications to more demanding systems. The results are summarized in Table 1 as well as several figures. Some of the underlying tools which have been developed or integrated in the individual steps appear to be quite powerful. For example, the localization of the "first" $CI_1^{0,1}$ at the perpendicular geometry ($\varphi^{0,1} = \pi/2$) has been achieved by means of the method based on the Longuet-Higgins theorem.[33] This requires nothing but quantum chemistry calculations of four "anchors" (the potential minima and two transition states) of C_5H_4NH in the electronic ground state S_0. Nevertheless, this rather restricted "input" from quantum chemistry, combined with the general results for the MS group, suffices in order to determine the global IREPs of all of the NACTs $\tau_k^{0,1}$ for the couplings of the PES of the electronic ground state V_0 and the excited state V_1, including all of the MS properties such as the nodal patterns and the signs of the NACTs or the opposite charges of the MS-adapted set of the two $CI_1^{0,1}$ and $CI_2^{0,1}$, and even the fact that the seam of $CI^{0,1}$ in the (r, φ)-plane is restricted to the orthogonal geometry, without any neccessity of calculating V_1 or the $\tau_k^{0,1}$ explicitly!

These and other, rather rich results for all of the NACTs and the CIs of the three lowest electronic singlet states S_1, S_1, and S_2 of C_5H_4NH have been confirmed by various tests for self-consistency. In particlar, we have calculated the **A** matrices for adiabatic-to-diabatic transformation, based on the MS-adapted NACTs, along different paths for molecular torsion. In the limit of torsion by 2π (360°), the **A** matrices approach the so-called topological matrices **D** which have to satisfy simple but mandatory quantization rules; i.e., they must be diagonal, with diagonal elements equal to 1 or −1 where the number of −1's must be even.[1] We consider the successful computational tests of this demanding rule as rewarding. Turning the table, the self-consistency tests could also be employed as alternative criteria for the determination of the IREPs; e.g., we could have used the information for the nodal patterns of the radial NACTs (Figure 7) instead of the switching property (Figure 6a); see the discusions in section III.

The present combination of quantum chemistry beyond Born−Oppenheimer and the molecular symmetry group suggests several extensions. First, the two fields should be combined with a third one, i.e., quantum reaction dynamics. The solutions of the corresponding time dependent Schrödinger equation, i.e., the representative wavepackets which are propagated on several coupled PES, depend on the couplings of the PES, i.e., on the NACTs. As a working hypothesis, these results should depend on the IREPs of the NACTs, in the frame of the MS group, if the wavepackets evolve from one molecular domain to different MS-adapted ones, e.g., due to large amplitude motions such as torsion or isomerization. For reference, effects of the MS group on the quantum reaction dynamics have been demonstrated previously, e.g., for laser separation of nuclear spin isomers,[45,46] but so far without explicit consideration of MS effects on the NACTs. Concerning the methodology, these quantum simulations should be carried out using the so-called diabatic representation, which is much more convenient than the adiabatic one.[1,2,28] It is gratifying that the present approach already provides the **A** matrix for the underlying adiabatic-to-diabatic transformation of the PES, based on the NACTs with proper IREPs. Second, we have implicitly assumed that the molecule is in the rotational ground state; this allowed us to use the MS-adapted torsional angle φ which describes the rotation of the light hydrogen atom of the NH bond relative to the heavy C_5H_4N fragment. For more general scenarios, the present approach should be extended to the theory of double groups.[47,48] Last but not least, it is a challenge to extend the present development to additional MS-adapted coordinates, and to molecules with more demanding MS groups, including groups with larger orders, and also with two- or more-dimensional IREPs; there are actually many systems in the literature which call for such extended investigations; see, e.g., refs 49 and 50. Work along these lines is in progress.

Acknowledgment. We thank Prof. Lluis Blancafort, Prof. Dietrich Haase, Prof. Yehuda Haas, PD Dr. Dirk Andrae, Mr. Thomas Grohmann, and Ms. Shireen Alfalah for advice and stimulating discussions, and Mr. Dominik Sattler for preparing Figures 1 and 2. This study was supported by the Deutsche Forschungsgemeinschaft in the framework of Project No. MA 515/22-2, and by Fonds der Chemischen Industrie.

Appendix

This Appendix considers the second example of section II, items vii and viii, in terms of symmetry-adapted Cartesian coordinates $s = \{x, y\}$, complementary to cylindrical coordinates $s = \{r, \varphi\}$. The scenario assumes that the first $CI_1^{i,i+1}$ has been discovered at $[s^{i,i+1}]_1 = [\{x^{i,i+1}, y^{i,i+1}\}]_1 = \{x, 0\}$. Application of the molecular symmetry operator (12)* generates the second $CI_2^{i,i+1}$ at $[\{x, y = 0\}]_2 = \{-x, 0\}$; see Figure 9. Here, we present a "shortcut" derivation of the opposite charges of $CI_1^{i,i+1}$ and $CI_2^{i,i+1}$, implying the IREP B_2 of $CI^{i,i+1}$, in accord with Table 1. For convenience, we use a simplified notation, by dropping many sub- or superscripts which the reader could add in accord with the rest of the paper.

A. Two (Symmetric) Two-State Conical Intersections in a Plane. We consider two two-state conical intersections, C_1 and C_2, located in a plane (see Figure 9). In addition, we distinguish between three regions: Λ_I, Λ_{II}, and Λ_0. Here, Λ_I is defined in terms of the closed contour L_I and contains the conical intersection C_1, Λ_{II} is defined in terms of the closed contour L_{II} and contains the conical intersection C_2, and Λ_0 is defined in terms of the closed contour L_0 and does not contain any ci. Next, for the sake of convenience, we assume all three contours to be rectangles. Consequently, we employ Cartesian coordinates: x and y (see Figure 9). Please note that the y-axis is defined along the line of symmetry. In what follows, we consider the two-state case and consequently concentrate on the following line

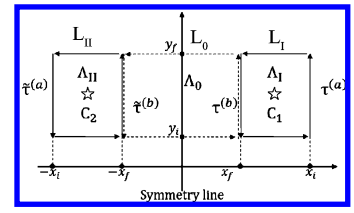

Figure 9. Two molecular-symmetry-adapted conical intersections C_1 and C_2 with the domains Λ_I and Λ_{II} encircled by closed loops L_I and L_{II} (continuous lines), respectively. The central domain Λ_0 surrounded by loop L_0 (dashed line) does not contain any CI. The arrows indicate the directions of integration for the corresponding contour integrals which are used to determine the charges of the conical intersections; see text.

integrals to calculate the corresponding topological (Berry) phase $\alpha(L)$:

$$\alpha(L) = \begin{cases} \oint_L \tau(s|L)\cdot \mathrm{d}s & (47a) \\ \oint_L \tau_s(s|L)\, \mathrm{d}s & (47b) \end{cases} \quad (47)$$

Here, $\tau(s|L)$ in eq 47a stands for the (1, 2) vectorial nonadiabatic coupling term (NACT) (the dot presents a scalar product) and $\tau_s(s|L)$ in eq 47b stands for the corresponding tangential component of $\tau(s|L)$:

$$\tau_s(s|L) = \langle \psi_i | \frac{\partial}{\partial s} \psi_{i+1} \rangle \quad (48)$$

and ds is an infinitesimal (scalar) distance along the contour. In the case of Cartesian coordinates s presents x and y. In what follows, we concentrate on eq 47b. Next, we make a few comments:

(a) Any line integral of the type given in eq 47, calculated along a closed contour that surrounds only one single ci, yields

$$\alpha(L) = \pm\pi \quad (49)$$

It is noticed that the value of the line integral is determined up to a sign.

(b) To treat the sign ambiguity in a more efficient way, it is suggested to extend eq 47b in the following way:

$$\alpha(L) = \oint_L e(s)|\tau_s(s|L)|\, \mathrm{d}s \quad (50)$$

so that the sign of the integrand along the contour L is determined by $e(s)$, where $e(s)$ is a function of s which is allowed to have two values only, namely, $e(s) = \pm 1$. It is positive when $\tau_s(s|L) > 0$ and negative when $\tau_s(s|L) < 0$ (thus $e(s)$ is a step function).

(c) The introduction of $e(s)$ is particularly convenient when the contour L is close enough to a given ci, e.g., C_j. It is well-known that in such a case $\tau_s(s|L_j)$ does not flip signs along the contour and therefore $e(s)$ keeps its sign constant along the whole contour so that:

$$\alpha_j(L_j) = \oint_{L_j} e(s)|\tau_s(s|L_j)|\, \mathrm{d}s = e_j \oint_{L_j} \tau_s(s|L_j)\, \mathrm{d}s = e_j\pi \quad (51)$$

with $j = 1, 2$. Equation 51 is an extension of eq 49.

(d) Any line integral of the type in eq 47 calculated for a *closed* contour that does not surround any conical intersection is zero (this follows from the existence of the two-state curl equation at each point in such a region; see, for instance, Chapter 1.3.2.2 in ref 1). From Figure 9, it can be seen that L_0 is such a (closed) contour and the corresponding line integral to be considered is

$$\alpha_0(L_0) = \oint_{L_0} e(s)|\tau_s(s|L_0)|\, \mathrm{d}s = 0 \quad (52)$$

B. Computation Applying Cartesian Coordinates. In what follows, we expand the line integrals in eqs 50, 51, and 52 employing Cartesian coordinates. Thus, any of the closed L contours (see Figure 9) are defined in terms of two horizontal lines $y = y_1$, y_2 and two perpendicular lines $x = x_1$, x_2 and consequently four (corner) points:

$$(x_1, y_1) \rightarrow (x_1, y_2) \rightarrow (x_2, y_2) \rightarrow (x_2, y_1) \rightarrow (x_1, y_1) \quad (53)$$

where the last point is identical to the first. As for $\tau(x,y|L)$, its two (planar) Cartesian components are (τ_x, τ_y). To continue, we consider the rhs line integral in eq 51 (namely, the line integral that surrounds C_1, see Figure 9):

$$\alpha(L_1) = e_1\{ \int_{y_i}^{y_f} \mathrm{d}y' \tau_y(x_i, y') + \int_{x_i}^{x_f} \mathrm{d}x' \tau_x(x', y_f) + \int_{y_f}^{y_i} \mathrm{d}y' \tau_y(x_f, y') + \int_{x_i}^{x_f} \mathrm{d}x' \tau_x(x', y_i)\} \quad (54)$$

A similar result can be obtained for $\alpha(L_{II})$. To simplify the treatment, we assume that $\tau_x \sim 0$ (this is achieved if we let $y_i \rightarrow -\infty$ and $y_f \rightarrow +\infty$, and consequently the respective two x-components of τ become zero). Consequently, we are left with two terms in eq 54:

$$\alpha(L_1) = e_1\{ \int_{y_i}^{y_f} \mathrm{d}y' \tau_y(x_i, y') + \int_{y_f}^{y_i} \mathrm{d}y' \tau_y(x_f, y')\} \quad (55)$$

and a similar expression for $\alpha(L_{II})$. Next are introduced the following definitions (see Figure 9):

$$\begin{aligned} \tau^{(a)} &= \int_{y_i}^{y_f} \mathrm{d}y' \tau_y(x_i, y') \\ \tau^{(b)} &= \int_{y_f}^{y_i} \mathrm{d}y' \tau_y(x_f, y') \\ \tilde{\tau}^{(b)} &= \int_{y_i}^{y_f} \mathrm{d}y' \tau_y(-x_f, y') \\ \tilde{\tau}^{(a)} &= \int_{y_f}^{y_i} \mathrm{d}y' \tau_y(-x_i, y') \end{aligned} \quad (56)$$

with two additional comments:

(i) Since all of the τ_y's are calculated along segments close to one of the cis, their values are always positive.

(ii) Although eq 56 presents four different line integrals, namely, $\tau^{(a)}$, $\tau^{(b)}$, $\tilde{\tau}^{(a)}$, and $\tilde{\tau}^{(b)}$, we have, due to symmetry (see Figure 9), two identical pairs, namely, $\tau^{(a)} = \tilde{\tau}^{(a)}$ and $\tau^{(b)} = \tilde{\tau}^{(b)}$.

Next, we evaluate eq 55 for the two relevant rectangles Λ_I and Λ_{II}:

(I) For Λ_I, we have

$$\alpha(L_I) = e_1(\tau^{(a)} + \tau^{(b)}) = e_1\pi \quad (57)$$

This result follows from the fact that both segments $x = x_i$ and $x = x_f$ are close enough to C_1 (see also eq 51 for $j = 1$).

(II) For Λ_{II}, we have (a similar result):

$$\alpha(L_{II}) = e_2(\tilde{\tau}^{(a)} + \tilde{\tau}^{(b)}) \equiv e_2(\tau^{(a)} + \tau^{(b)}) = e_2\pi \quad (58)$$

This result follows from the fact that both segments $x = -x_i$ and $x = -x_f$ are close enough to C_2 (see also eq 51 for $j = 2$).

(III) For Λ_0, the situation is somewhat more complicated. Employing, again, the Cartesian coordinates, recalling that all $\tau_x \sim 0$ and that the τ_y's do not flip signs along $x = x_f$, $-x_f$, we get that

$$\alpha(L_0) = \{ \int_{y_i}^{y_f} dy' \tau_y(x_f, y') e(x_f, y') + \int_{y_f}^{y_i} dy' \tau_y(x_f, y') e(-x_f, y') \} \quad (59)$$

Next, since the segment $x = +x_f$ is close to C_1 and the segment $x = -x_f$ is close to C_2, we get that $e(x_f, y) \sim e_1$ (for any y-value) and $e(-x_f, y) \sim e_2$, so that eq 59 becomes

$$\alpha(L_0) \sim (e_1 \tau^{(b)} + e_2 \tilde{\tau}^{(b)}) = \tau^{(b)}(e_1 + e_2) = 0 \quad (60)$$

The only way eq 60 can yield the value of zero is to require that $e_2 = -e_1$. This outcome implies that the two cis, namely, C_1 and C_2, are formed by two identical NACTs but with opposite signs (charges). If the two corresponding NACTs are characterized by two well-defined pronounced peaks, this result implies that the two peaks are of opposite signs. A byproduct of this proof is that

$$\alpha(L_I) = -\alpha(L_{II}) \quad (61)$$

See eqs 57 and 58.

References and Notes

(1) Baer, M. *Beyond Born Oppenheimer: Electronic non-Adiabatic Coupling Terms and Conical Intersections*; Wiley & Sons Inc: Hoboken, NJ, 2006.

(2) Domcke, W., Yarkony, D. R., Köppel, H., Eds. *Conical Intersections: Electronic Structure, Dynamics and Spectroscopy*; World Sci.: Singapore, 2004.

(3) Levine, B. J.; Martinez, T. J. *Annu. Rev. Phys. Chem.* **2007**, *58*, 613.

(4) Barbatti, M.; Belz, S.; Leibscher, M.; Lischka, H.; Manz, J. *Chem. Phys.* **2008**, *350*, 145.

(5) Abe, M.; Ohtsuki, Y.; Fujimura, Y.; Lan, Z.; Domcke, W. *J. Chem. Phys.* **2006**, *124*, 224316.

(6) Mead, C. A. *Chem. Phys.* **1980**, *49*, 23, 33.

(7) Wu, Y-S. M.; Kuppermann, A. *Chem. Phys. Lett.* **1993**, *201*, 178; **1995**, *235*, 105.

(8) Bunker, P. R.; Jensen, P.; *Molecular Symmetry and Spectroscopy*; NRC Research Press: Ottawa, Canada, 1998.

(9) Baer, M.; Billing, G. D. The Role of Degenerate States in Chemistry. *Adv. Chem. Phys.* **2002**, *124*. In particular, see: (a) Child, M. S. p 1. (b) Adhikari, S.; Billing, G. D. p 143. (c) Englman, R.; Yahalom, A. p 197. (d) Kuppermann, A.; Abrol, R. p 323. (e) Worth, G. A.; Robb, M. A. p 355.

(10) Kuppermann, A.; *Dynamics of Molecules and Chemical Reactions*; Wyatt, R. E., Zhang, Z. H., Eds.; Marcel: New York, 1996; p 411.

(11) Halász, G. J.; Vibók, Á.; Baer, R.; Baer, M. *J. Phys. A* **2007**, F267.

(12) (a) Baer, R.; Charutz, D. M.; Kosloff, R.; Baer, M. *J. Chem. Phys.* **1996**, *105*, 9141. (b) Adhikari, S; Billing, G. D. *J. Chem. Phys.* **1999**, *111*, 40.

(13) (a) Baer, M.; Vertesi, T.; Halasz, G. J.; Vibok, A.; Suhai, S. *Faraday Discuss.* **2004**, *127*, 337. (b) Halász, G. J.; Vibók, Á; Suhai, S.; Baer, M. *J. Chem. Phys.* **2007**, *127*, 244101.

(14) Halász, G. J.; Vibók, Á.; Baer, R.; Baer, M. *J. Phys. A: Math. Theor.* **2007**, *40*, F267.

(15) Halász, G. J.; Vibók, Á.; Hoffman, D. K.; Kouri, D. J.; Baer, M. *J. Chem. Phys.* **2007**, *126*, 154309.

(16) (a) Sadykov, R. G.; Yarkony, D. R. *J. Chem. Phys.* **1998**, *109*, 20. (b) Yarkony, D. R. *J. Chem. Phys.* **2001**, *114*, 2614.

(17) Mead, C. A.; Truhlar, D. G. *J. Chem. Phys.* **1982**, *77*, 6090. Mead, C. A. *J. Chem. Phys.* **1983**, *78*, 807.

(18) Davidson, E. R. *J. Am. Chem. Soc.* **1977**, *99*, 397.

(19) (a) Barragan, P.; Errea, L. F.; Macias, A.; Mendez, L.; Riera, A.; Lucas, J. M.; Aguilar, A. *J. Chem. Phys.* **2004**, *121*, 11629. (b) Sevryuk, M. B.; Rusin, L. Y.; Cavalli, S.; Aquilanti, V. *J. Phys. Chem. A* **2004**, *108*, 8731.

(20) (a) Englman, R.; Vertesi, T. *Phys. Lett. A* **2006**, *354*, 196. (b) Vertesi, T.; Englman, R. *J. Phys. B* **2008**, *41*, 025102.

(21) (a) Amaran, S.; Kumar, S. *J. Chem. Phys.* **2008**, *128*, 154325. (b) Amaran, S.; Kumar, S.; Köppel, H. *J. Chem. Phys.* **2008**, *128*, 124305. (c) Gomez-Carrasco, S.; Aquado, A.; Paniaqua, M.; Roncero, O. *J. Chem. Phys.* **2006**, *125*, 104105.

(22) (a) Hu, C.; Hirai, H.; Sugino, O. *J. Chem. Phys.* **2008**, *128*, 144111. (b) Hu, C.; Hirai, H.; Sugino, O. *J. Chem. Phys.* **2007**, *127*, 064103.

(23) (a) Gadea, X.; Pellisier, M. *J. Chem. Phys.* **1990**, *93*, 545. (b) Romero, T.; Aguilar, A.; Gedea, X. *J. Chem. Phys.* **1999**, *110*, 6219. (c) Mozhayskiv, V. A.; Babikov, D.; Krylov, A. I. *J. Chem. Phys.* **2006**, *124*, 224309.

(24) (a) Abrahamsson, E.; Groenenboom, G. C.; Krems, R. V. *J. Chem. Phys.* **2007**, *126*, 184309. (b) Rozgonyi, T.; González, L. *J. Phys. Chem. A* **2008**, *112*, 5573.

(25) (a) Puzari, P.; Sarkar, B.; Adhikari, S. *J. Chem. Phys.* **2004**, *121*, 707. (b) Sarkar, B.; Adhikari, S. *J. Chem. Phys.* **2006**, *124*, 074101.

(26) Godsi, P. O.; Evenhuis, C. R.; Collins, M. *J. Chem. Phys.* **2006**, *125*, 164321.

(27) (a) Kryachko, E. S.; Varandas, A. J. C. *Int. J. Quantum Chem.* **2002**, *89*, 255. (b) Kryachko, E. S. *Adv. Quantum Chem.* **2003**, *44*, 119. (c) Varandas, A. J. C.; Xu, Z. R. *Int. J. Quantum Chem.* **2004**, *99*, 385.

(28) (a) Baer, M. *Chem. Phys. Lett.* **1975**, *35*, 112. (b) Baer, M. *Mol. Phys.* **1980**, *40*, 1011.

(29) Baer, M.; Lin, S. H.; Alijah, A.; Adhikari, S.; Billing, G. D. *Phys. Rev. A* **2000**, *62*, 032506.

(30) (a) Levi, C.; Halász, G. J.; Vibók, Á.; Bar, I.; Zeiri, Y.; Kosloff, R.; Baer, M. *J. Chem. Phys.* **2008**, *128*, 244302. (b) Levi, C.; Halász, G. J.; Vibók, Á.; Bar, I.; Zeiri, Y.; Kosloff, R.; Baer, M. *Int. J. Quantum Chem.* **2009**, *109*, 2482.

(31) Slanina, Z. *Adv. Quantum Chem.* **1981**, *13*, 89.

(32) Longuet-Higgins, H. C. *Proc. R. Soc. London, Ser. A* **1975**, *344*, 147.

(33) Herzberg, G.; Longuet-Higgins, H. C. *Discuss. Faraday Soc.* **1963**, *35*, 77.

(34) Zilberg, S.; Haas, Y. *J. Phys. Chem. A* **2003**, *107*, 1222.

(35) Zilberg, S.; Haas, Y. *Adv. Chem. Phys.* **2002**, *124*, 433.

(36) Haas, Y.; Cogan, S.; Zilberg, S. *Int. J. Quantum Chem.* **2005**, *102*, 961.

(37) Berry, M. V. *Proc. R. Soc. London, Ser. A* **1984**, *392*, 45.

(38) Alfalah, S.; Belz, S.; Deeb, O.; Leibscher, M.; Manz, J.; Zilberg, S. *J. Chem. Phys.* **2009**, *130*, 124318.

(39) Haas, Y.; Zilberg, S. *Adv. Chem. Phys.* **2002**, *124*, 433.

(40) Roos, B. O. *Adv. Chem. Phys.* **1987**, *69*, 399.

(41) Granovsky, A. A. PC GAMESS, version 7.0, http://classic.chem.msu.su/gran/games/index.html.

(42) MOLPRO is a package of ab initio programs written by Werner, H.-J.; Knowles, P. J.; Lindh, R.; Manby, F. R.; Schütz, M.; Celani, P.; Korona, T.; Rauhut, G.; Amos, R. D.; Bernhardsson, A.; Berning, A.; Cooper, D. L.; Deegan, M. J. O.; Dobbyn, A. J.; Eckert, F.; Hampel, C.; Hetzer, G.; Lloyd, A. W.; McNicholas, S. J.; Meyer, W.; Mura, M. E.; Nickla A.; Palmieri, P.; Pitzer, R.; Schumann, U.; Stoll, H.; Stone, A. J.; Tarroni, R.; Thorsteinsson, T.

(43) Mebel, A. M.; Baer, M.; Lin, S. H. *J. Chem. Phys.* **2001**, *114*, 5109.

(44) Mebel, A. M.; Yahalom, A.; Englman, R.; Baer, M. *J. Chem. Phys.* **2001**, *115*, 3673.

(45) Grohmann, T.; Deeb, O.; Leibscher, M. *Chem. Phys.* **2007**, *338*, 252.

(46) Deeb, O.; Leibscher, M.; Manz, J.; von Muellern, W.; Seideman, T. *ChemPhysChem* **2007**, *8*, 322.

(47) Soldan, P. *J. Math. Chem.* **1996**, *20*, 331.

(48) Hougen, J. T.; Dekoven, B. M. *J. Mol. Spectrosc.* **1983**, *98*, 375.

(49) Poisson, L.; Raffael, K. D.; Soep, B.; Mestdagh, J. M.; Buntinx, G. *J. Am. Chem. Soc.* **2006**, *126*, 10.

(50) Poisson, L.; Roubin, P.; Coussan, S.; Soep, B.; Mestdagh, J. M. *J. Am. Chem. Soc.* **2008**, *130*, 10.

JP905038T